

Universidade de Brasília - UnB
Faculdade UnB Gama - FGA
Gas Dynamics

Numerical Simulation of the Supersonic Diffuser and Nozzle

Luso de Jesus Torres

Brasília, DF

2021



Sumário

1	INTRODUCTION	3
I	PLANAR SUPERSONIC DIFFUSER	4
2	THEORETICAL PARAMETERS	5
3	CONVERGENCE ANALYSIS FOR THE DIFFUSER	7
4	DIFFUSER SETUP	9
4.1	Mesh Settings	9
4.2	Mesh Quality	10
4.3	Fluent Setup	13
4.3.1	Viscous Flow modifications	15
5	METHODS	16
6	RESULTS OF PART I	17
6.1	Inviscid Part	17
6.2	Viscous Part	20
7	DISCUSSION OF RESULTS OF PART I	26
II	CONICAL AND BELL-SHAPED NOZZLES	28
8	GEOMETRY DESCRIPTION	29
9	NOZZLE SETUP	31
9.1	Mesh Settings	31
9.2	Mesh Quality	32
9.3	Fluent Setup	35
9.3.1	Viscous Flow modifications	37
10	RESULTS OF PART II	39
10.1	Bell-Shaped Nozzle	39
10.1.1	Inviscid Part	39
10.1.2	Viscous	42
10.2	Conical-Shaped Nozzle	45

10.2.1	Inviscid	45
10.2.2	Viscous	48
11	DISCUSSION OF RESULTS OF PART II	51
11.1	Bell-Shaped	51
11.2	Conical-Shaped Nozzle	52
12	CONCLUSION	54
	REFERENCES	55

1 Introduction

The present work pursues to validate the optimal geometries obtained in work 1 being part I advocated to the diffuser and in part II the nozzles will be validated according to their inviscid and viscous behavior.

All simulations performed in this document will be represented with the tools disposed by ANSYS, in the CFD application FLUENT.

Part I

Planar Supersonic Diffuser

2 Theoretical Parameters

The first part of this work consists in analysing the theoretical values obtained with help of the Shock Wave Theory, being such parameters Mach Number, static Pressure, Temperature, Velocity and Density, resumed in Table 1.

The supersonic diffuser proposed in work 1 was designed to operate with maximum efficiency at Mach 3.5 and an equivalent altitude of 22 km. Figures 1 and 2 shows the intended configuration and the obtained geometry in CATIA V5R19 respectively. The angles and the diameter were calculated in (TORRES, 2021) based on the parameters from Table 2.

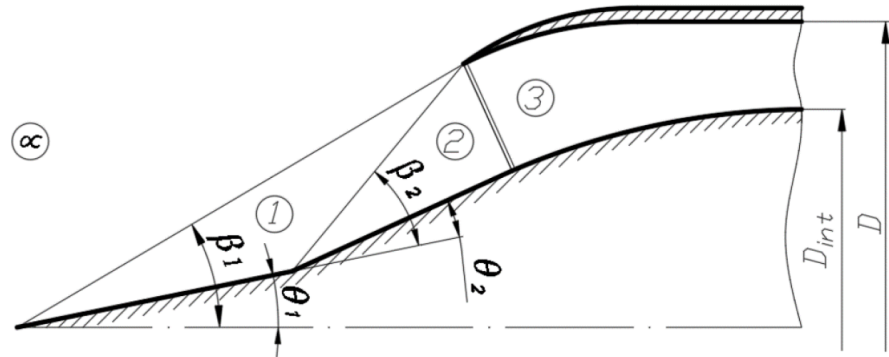


Figura 1 – Supersonic Diffuser Geometry

Parameter \ Station	0 (∞)	1	2	3
Mach Number	3.5	2.55	1.65	0.66
Static Pressure [kPa]	5.47	18.58	63.02	189.12
Temperature [K]	216.65	325.82	489.97	701.21
Velocity [km/s]	1.03	0.93	0.73	0.35
Density [kg/m ³]	0.09	0.20	0.45	0.94

Tabela 1 – Design Parameters for each Station. Source: (TORRES, 2021)

Property	Value
β_1 [deg]	29.90
β_2 [deg]	43.10
θ_1 [deg]	15.60
θ_2 [deg]	20.57
$\left(\frac{P_{0,e}}{P_{0,i}}\right)$	0.62
D [kN]	1716.5

Tabela 2 – Expected angles, efficiency and Drag. Source: (TORRES, 2021)

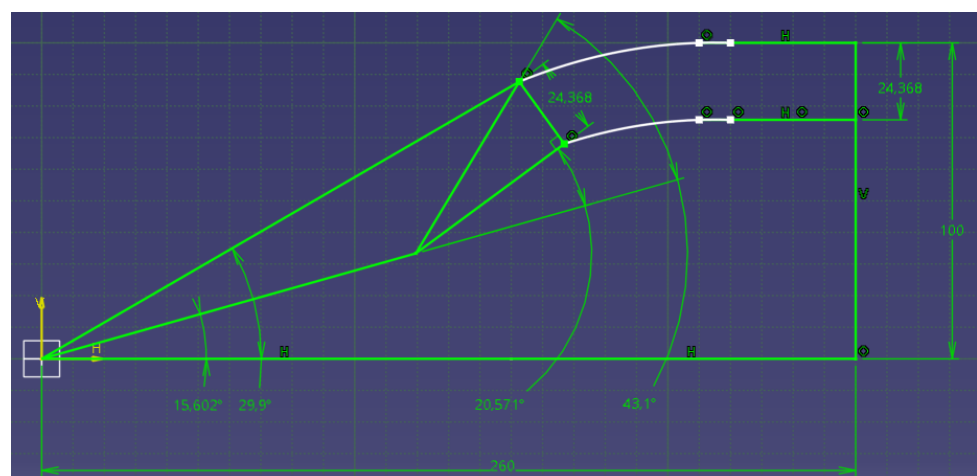


Figura 2 – Initial Diffuser Design. Source: ([TORRES, 2021](#))

3 Convergence Analysis for the Diffuser

To validate the analytical results, a convergence analysis was made based on the formation of shock waves in the desired position, and finally was established the length D_{int} in terms of the presence of a normal shock wave at the inlet of station 3. The sketches were made in ANSYS Design Modeler.

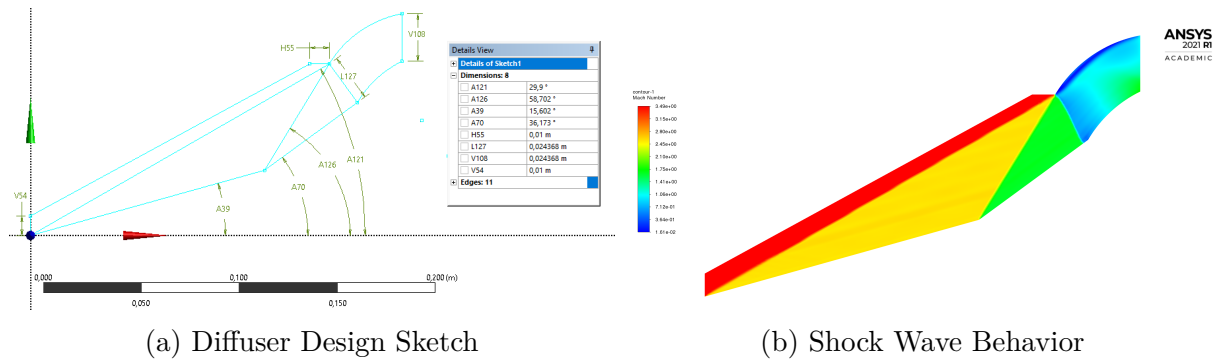


Figure 3 – Non-Tangent Configuration

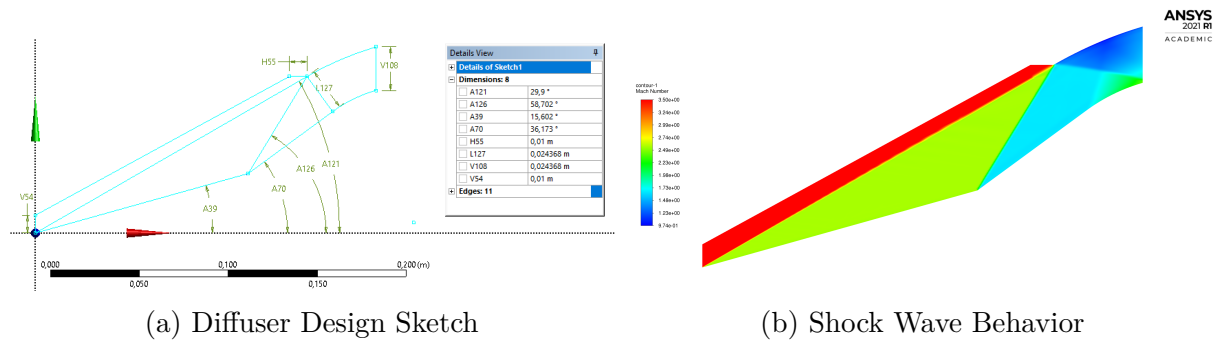


Figure 4 – Tangent Configuration with Constant Area

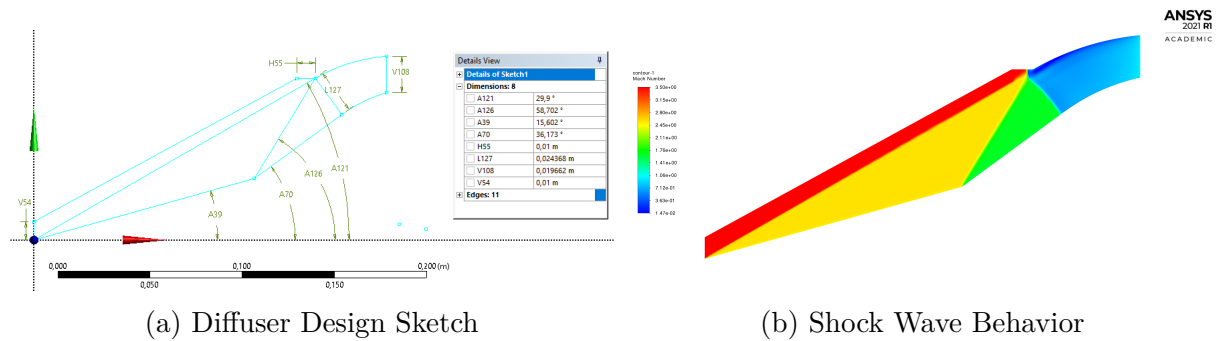


Figure 5 – Tangent Configuration with Decreasing Area

Based on what was observed during each simulation, the normal shock wave formed at the inlet of the diffuser has a relation with the internal Diameter D_{int} and the

smoothness inside the diffuser. A tangent surface is completely necessary to have flow field continuity inside the device and the exit length has to be somewhere between 3/4 of the inlet length. The ratio obtained for these two measurements was 0.8069 for the proper normal shock wave behavior at station 3.

The final geometry is presented below in Figure 6:

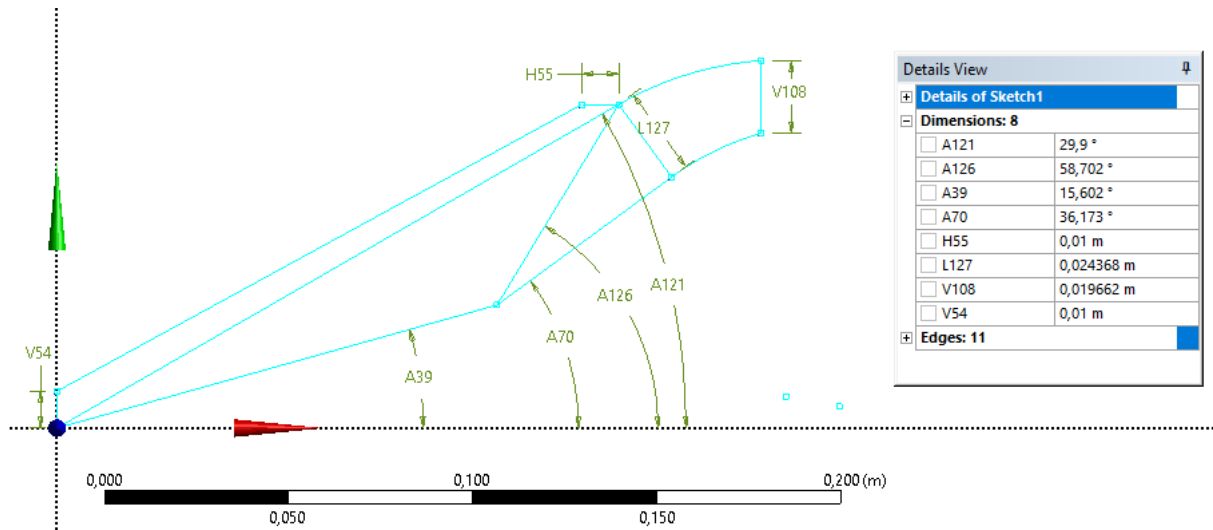


Figure 6 – Diffuser Final Configuration

4 Diffuser Setup

To validate our analytical model, both the inviscid and viscous flow will be considered. For promotion of concrete simulation models of our analytical problem, two different metrics will be discussed and the respective results will be illustrated.

4.1 Mesh Settings

Both meshes created are made from the functions *Face Meshing* and *Sizing* depending on the demand of the simulation results.

For the inviscid case, the geometry has only mesh refinement in the vertical edges of the inlet and outlet, where the number of elements is presented besides the geometry, as shown in Figure 7.

In the case of the viscous model, a more refined mesh was created attempting to obtain better results near the walls of our structure, as shown in Figure 8. To do this, the tool *FaceSplit* created both surfaces from the original sketch.

Even though from the illustration presented in Figure 8, which can be translated to an increase in the density of cells next to the inlet and outlet of both diffusers, it was necessary to obtain higher precision next to the station 3 and the walls of the device in the case of the viscous flow.

This is done by dividing even further the number of divisions next to the walls and splitting the surface into 2 different regions. Therefore, both figures illustrates the number of elements and nodes inside the geometries to specify the difference among them.



Figure 7 – Mesh for the Diffuser with inviscid flow.

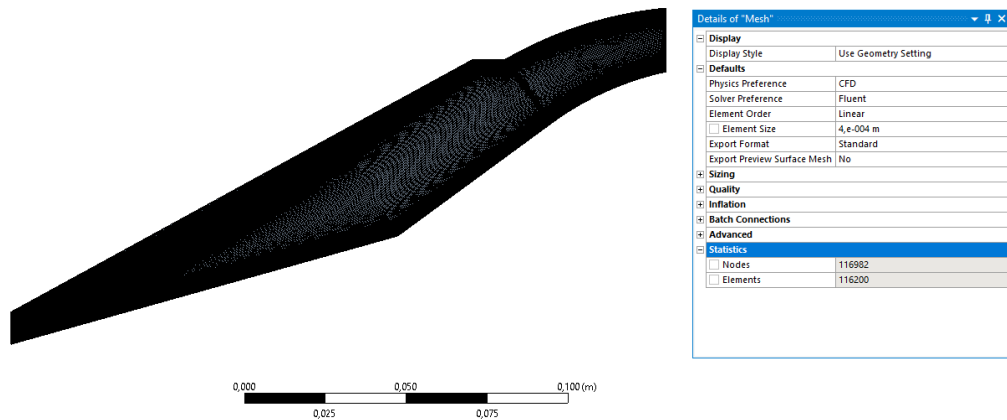
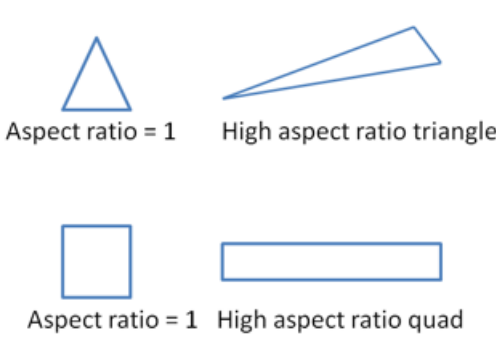


Figure 8 – Mesh for the Diffuser with viscous flow.

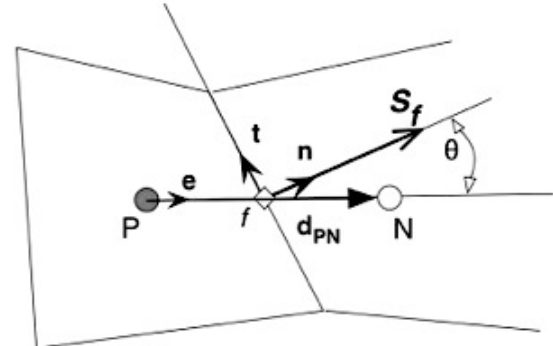
4.2 Mesh Quality

To qualify the previous presented meshes, two different metrics are proposed. The first method is the Aspect Ratio, which characterizes the ratio between the major and minor edge of a mesh element. (LUIZ, 2015) Ideally, the aspect ratio must be 1, i.e., a better symmetry of edges to guarantee better results. Two examples are illustrated in Figure 9a.

In the same manner as the metric Aspect Ratio, Orthogonality quantify the deviation of the angle between the vector connecting adjacent cells centroid and the vector normal to the cell surface and their faces (LUIZ, 2015). Is one of the best measurements to penalize the gradient operator in a mesh. Figure 9b illustrates the idea behind the metric.



(a) Aspect Ratio



(b) Orthogonality

Figure 9 – Selected metrics to validate the Meshes. Source: (LUIZ, 2015)

The results are shown below on Figures 10 and 11 for the inviscid flow.

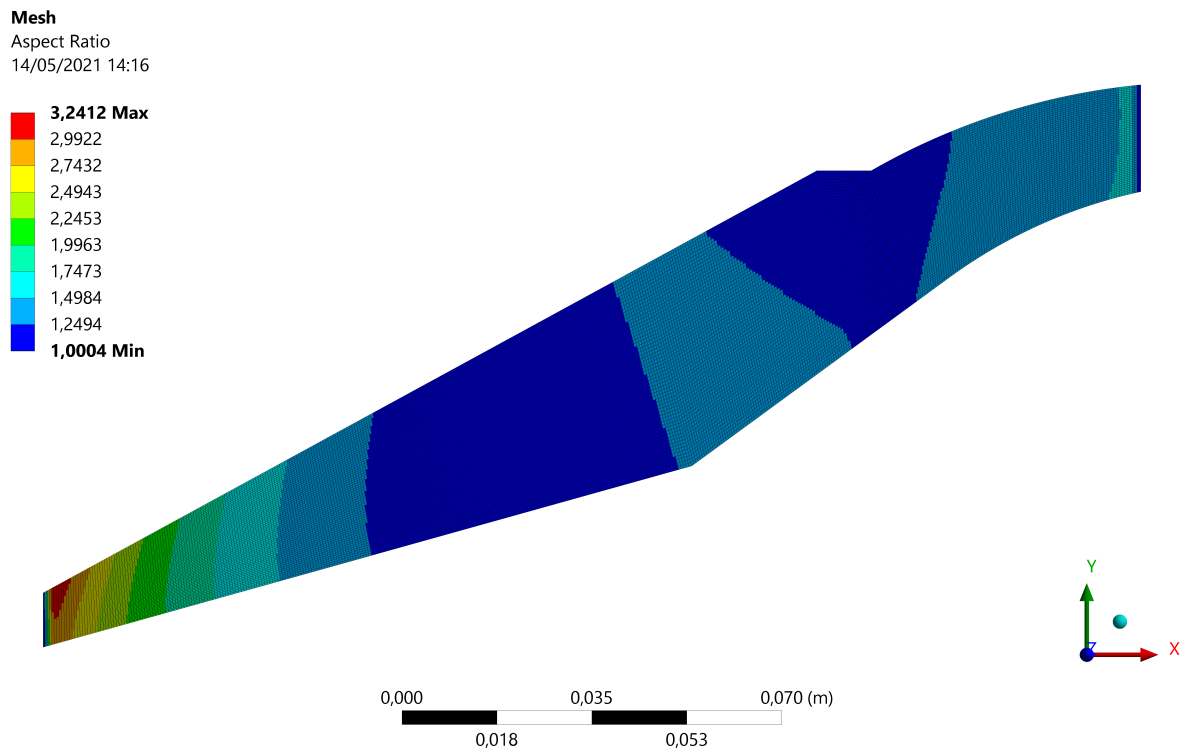


Figure 10 – Mesh quality for Aspect Ratio Metric for the inviscid geometry.

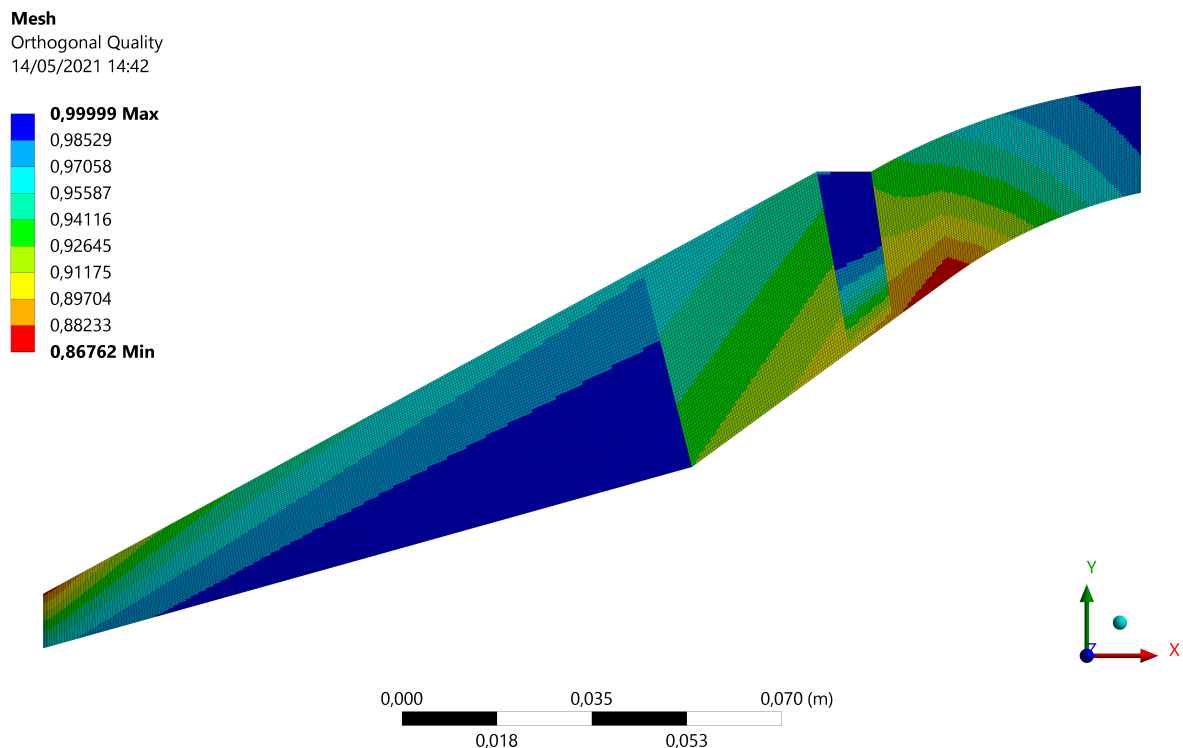


Figure 11 – Mesh quality for Orthogonality Metric for the inviscid geometry.

The meshes presented are sufficient to satisfy our simulation, since next to the regions of the quality problems are not that relevant for the inviscid flow, and are not

even below values to be root of calculation errors, since for orthogonality the error is expected to be less 14% and for the aspect ratio, an issue is only on the constant inlet values, making them negligible. The following results apply for the viscous geometry.

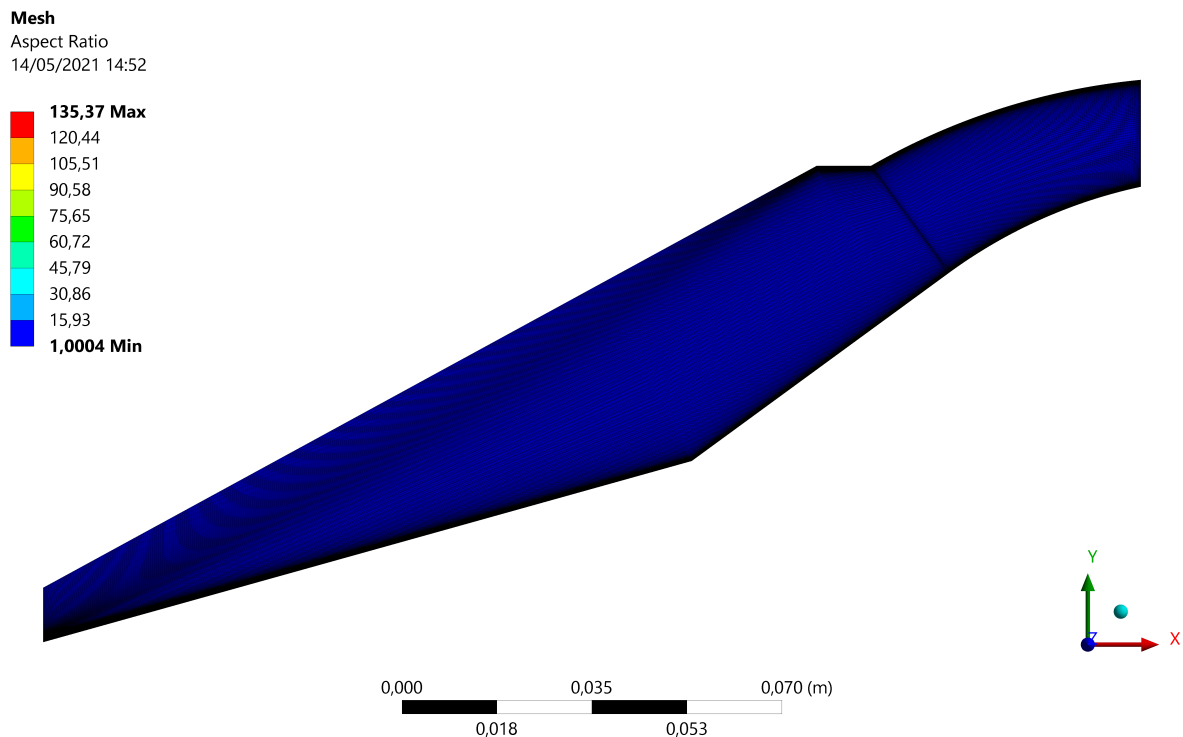


Figure 12 – Mesh quality for Aspect Ratio Metric for the viscous geometry.

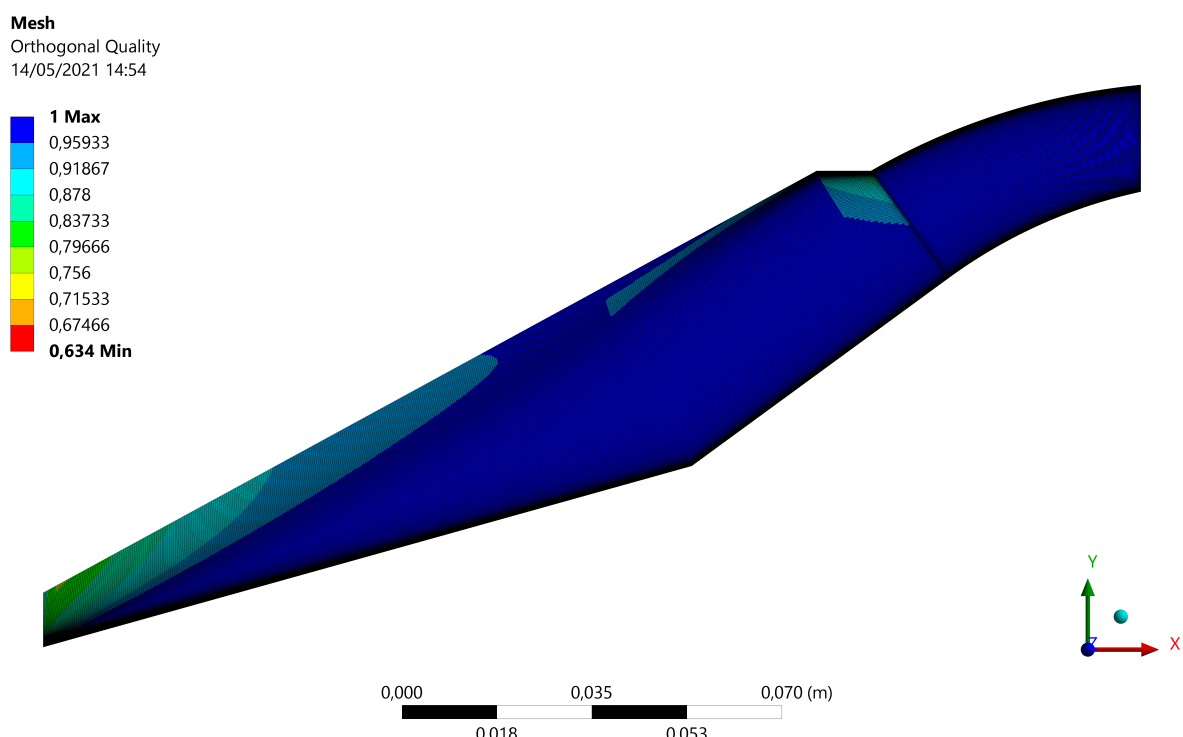


Figure 13 – Mesh quality for Orthogonality Metric for the viscous geometry.

The effects of quality for both Figures 10 and 11 are corrected in 12 13 for more rigorous analysis of the flow next to the surfaces of our device. The result presented has elevated computational complexity as a downside.

The next sections will present the results obtained for inviscid and viscous flows.

4.3 Fluent Setup

From the panel on ANSYS Fluent (Figure 60), the following set of configurations was modified:

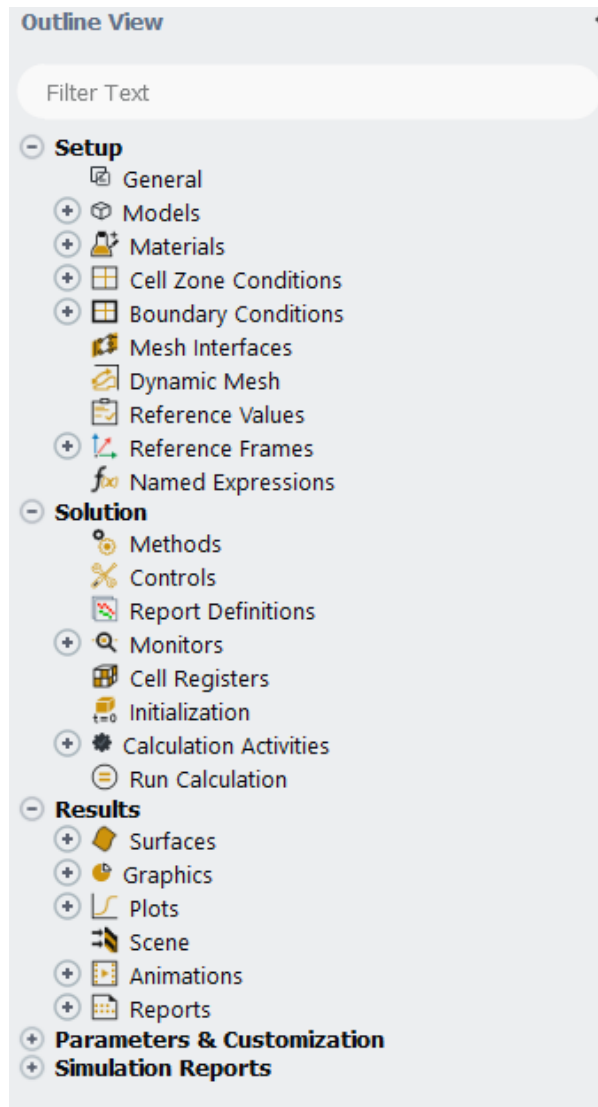


Figure 14 – Ansys Fluent Panel

Setup -> General: From *Pressure Based* to *Density Based*;

Setup -> Models: *Energy* (On) / *Viscous* (Inviscid);

Setup -> Materials -> Fluid -> air : *Density* (ideal-gas);

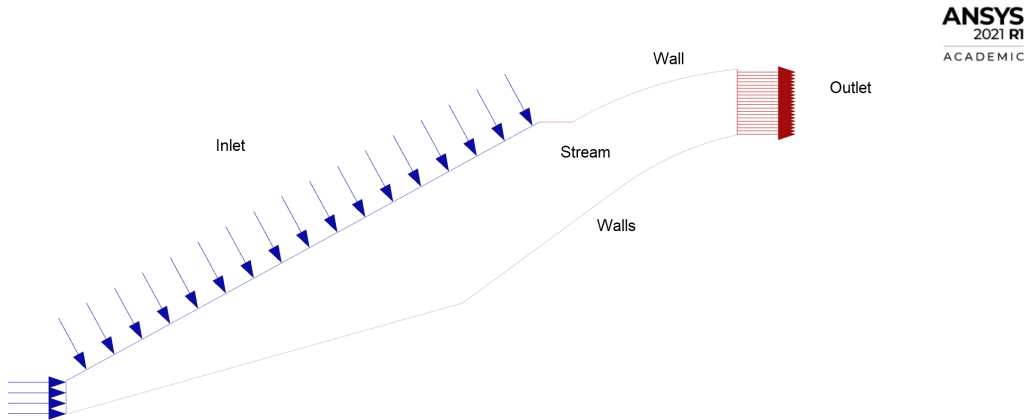


Figure 15 – Boundary Conditions: Diffuser.

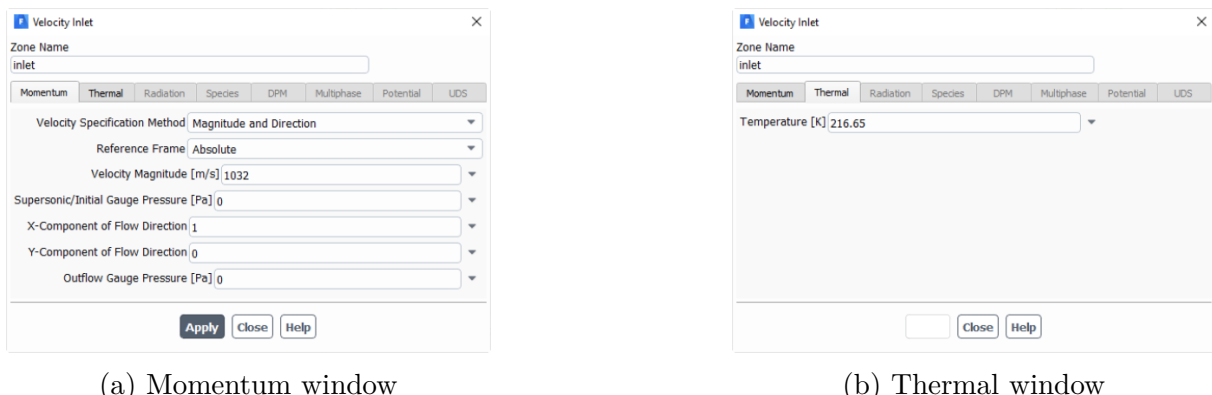


Figure 16 – Boundary Conditions: Inlet

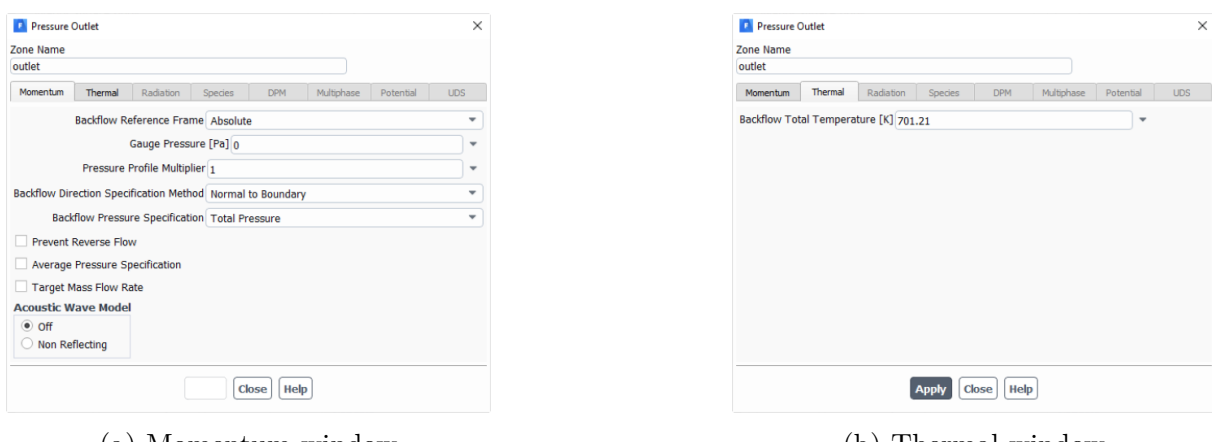


Figure 17 – Boundary Conditions: Outlet

To clarify the boundary conditions, Figure 15 will serve as a reference.

Setup -> Boundary Conditions -> Inlet : Figure 16 contains the settings;

Setup -> Boundary Conditions -> Outlet : Figure 17 contains the settings, change the condition type to *Pressure Outlet*;

Setup -> Boundary Conditions -> Wall : Change *stream* condition type to *pressure-far-field*.

Solution -> Methods : *Flow* (First Order Upwind), this option was chosen to the simulation due to its stability and lower processing time. Inside the panel, in *High Order Term Relaxation* the *Relaxation Factor* was set 0.5 and the option *Variables* was changed to *all variables*;

Solution -> Controls : *Courant Number* 1.

Solution -> Initialization : Figure 18 contains the settings. Attention for the *Gauge Pressure* in the initialization (half the value at the inlet).

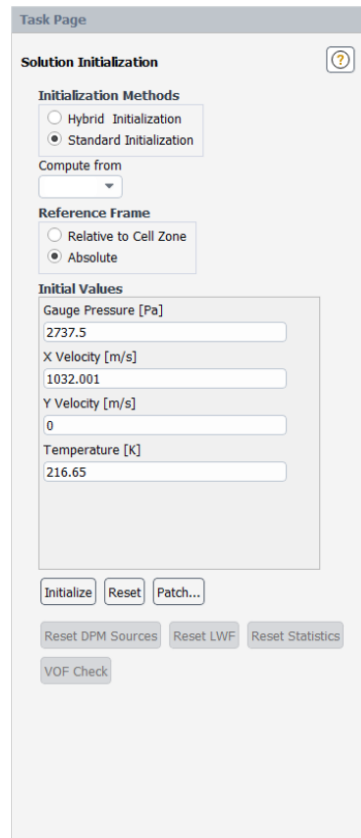


Figure 18 – Initialization window

4.3.1 Viscous Flow modifications

Setup -> Models: *Energy* (On) / *Viscous* (Spalart-Allmaras 1 eqn).

Some procedures as animating the solution and interpolating the data from the inviscid simulation to the viscous simulation can improve the processing time.

5 Methods

The method utilized to obtain the numeric properties in each section is based on the lines created in the geometry. Figure 19 show these lines.

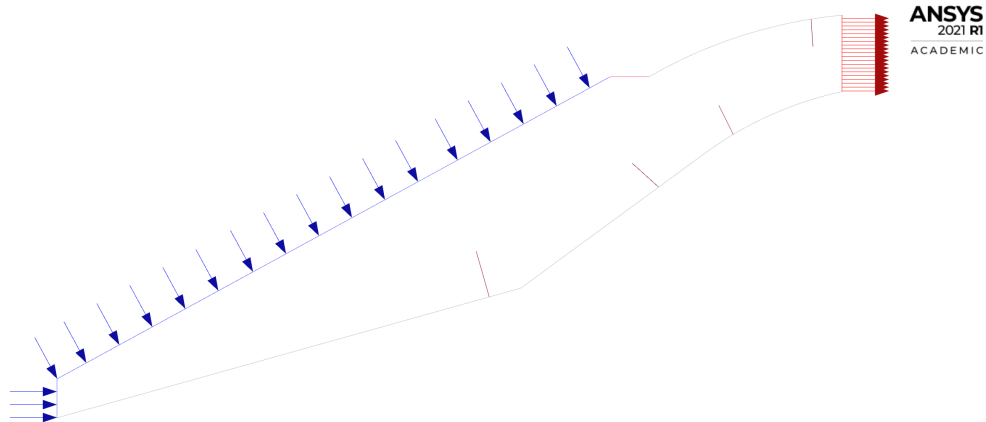


Figure 19 – Auxiliary lines to calculate property in each region

To make use of those lines, the following set of steps must be followed:

Results -> Reports -> Surface Integrals : Selecting *Area-Weighted Average*, the field variables will be available, as shown in Figure 20

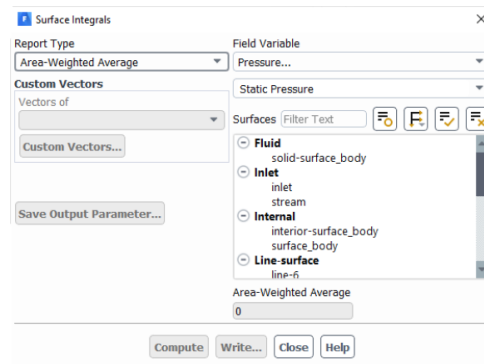


Figure 20 – Available Flow Properties in Surface Integrals

6 Results of Part I

6.1 Inviscid Part

The following set of Figures will describe the Inviscid Results (if necessary zoom in for better details in the graphs):

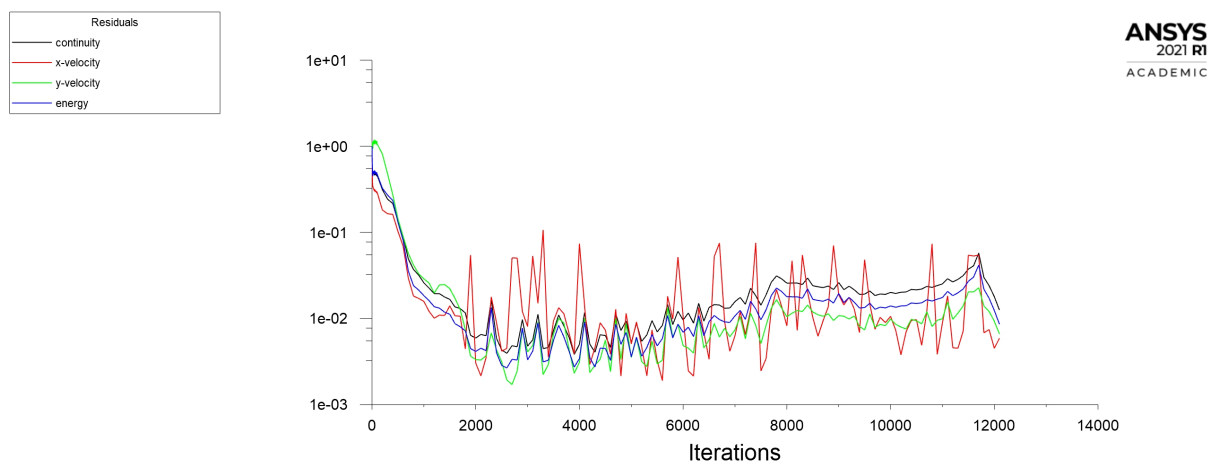


Figure 21 – Residuals for the inviscid simulation (12000 iterations)

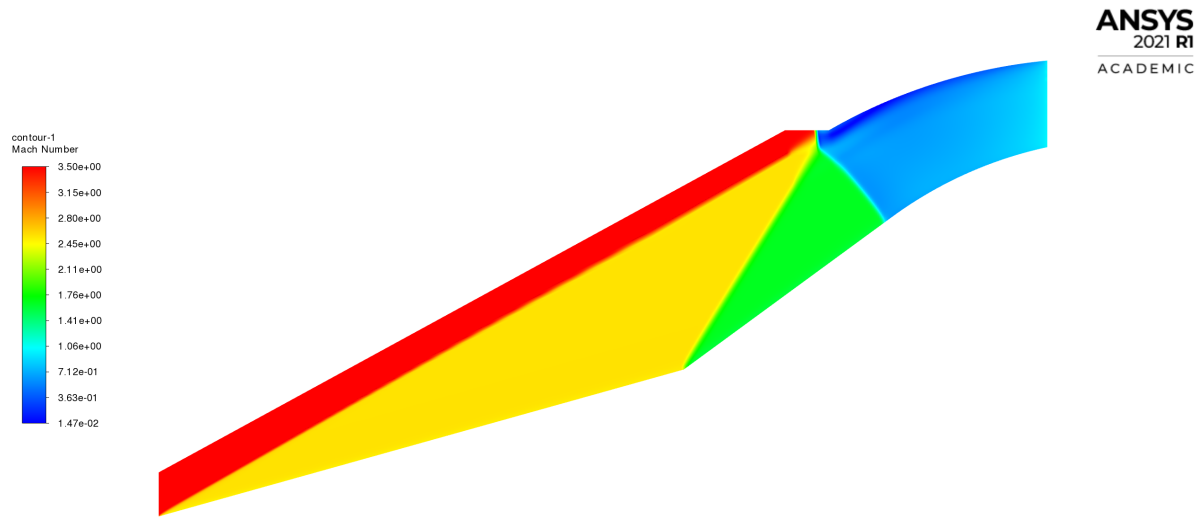


Figure 22 – Mach Number Field for the inviscid Flow

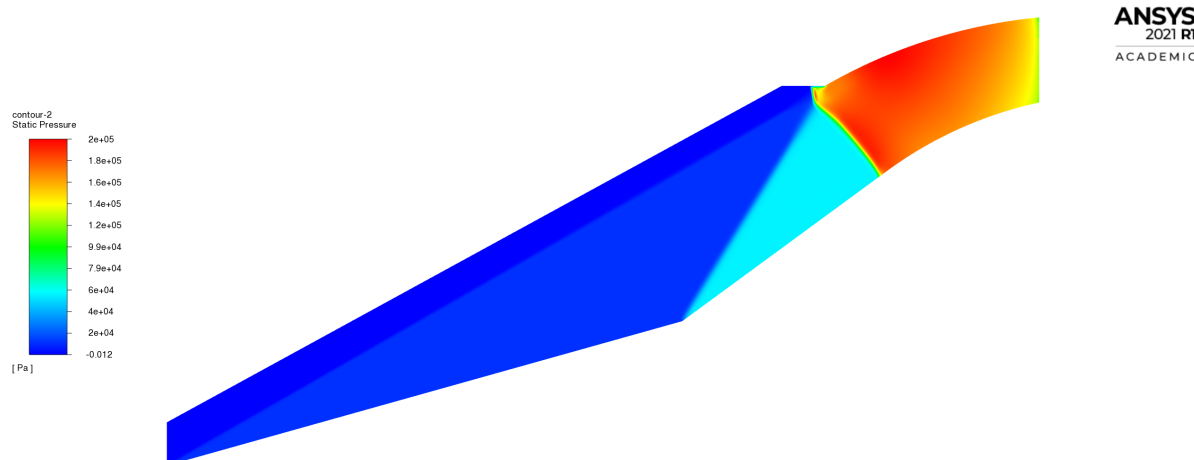


Figure 23 – Pressure Field for the inviscid Flow

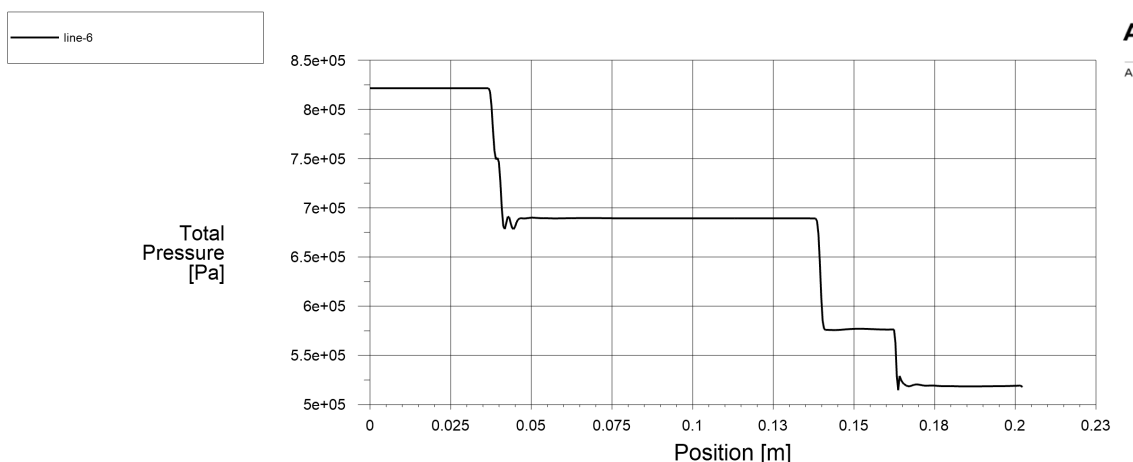


Figure 24 – Total Pressure Plot for the inviscid Flow

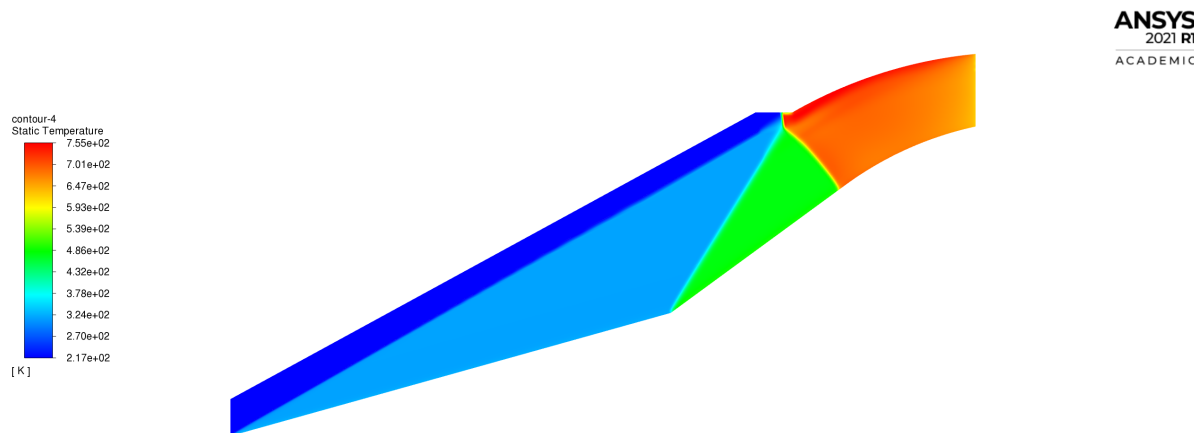


Figure 25 – Temperature Field for the inviscid Flow

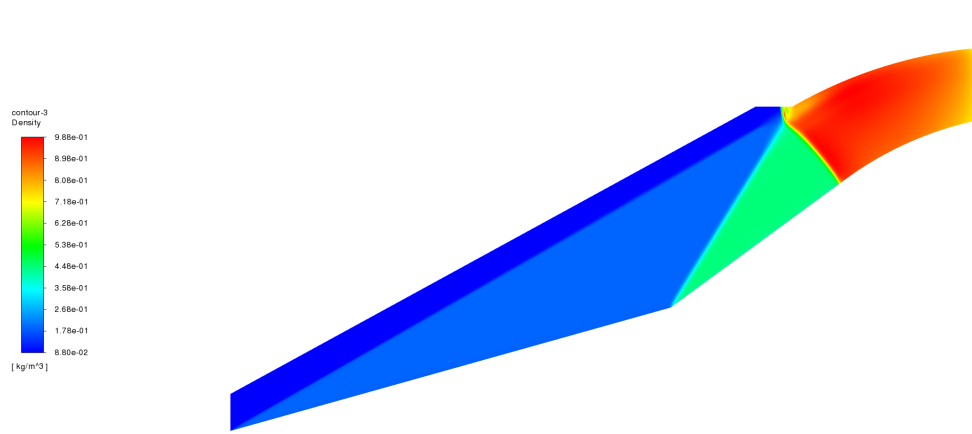
ANSYS
2021 R1
ACADEMIC

Figure 26 – Density Field for the inviscid Flow

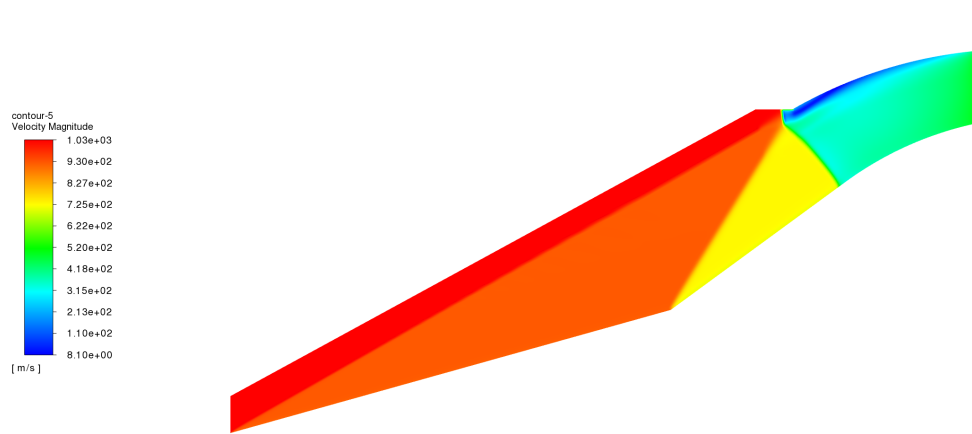
ANSYS
2021 R1
ACADEMIC

Figure 27 – Velocity Field for the inviscid Flow

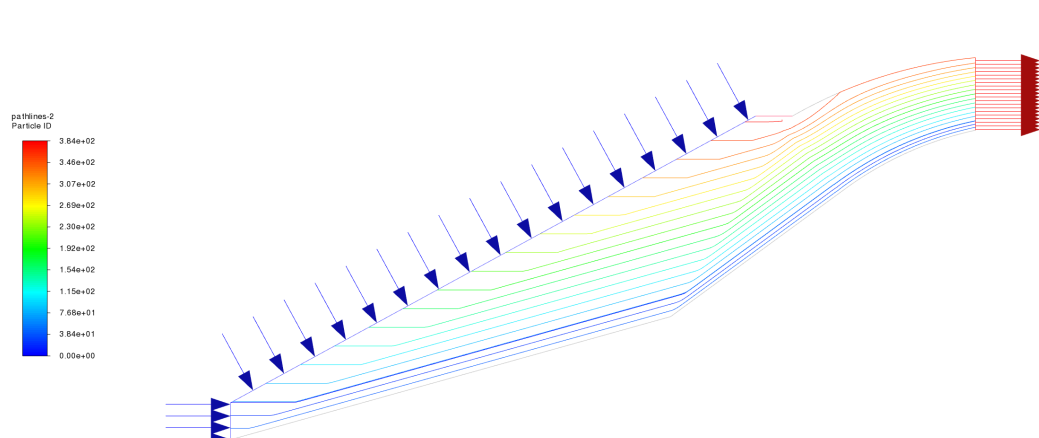
ANSYS
2021 R1
ACADEMIC

Figure 28 – Velocity path-lines for the inviscid Flow

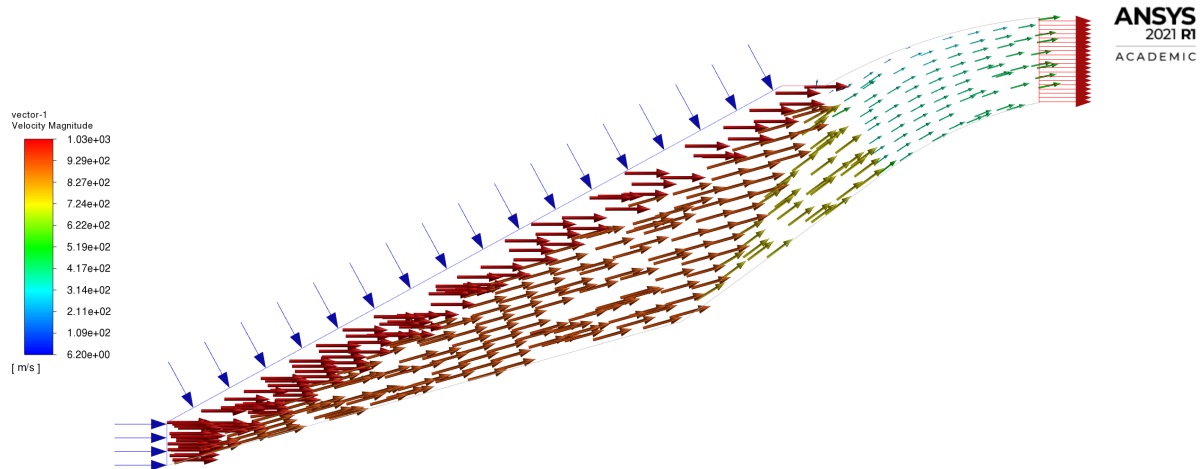


Figure 29 – Velocity Vectors for the inviscid Flow

6.2 Viscous Part

The following set of Figures will describe the Viscous Results (If necessary zoom in for better details in the graphs):

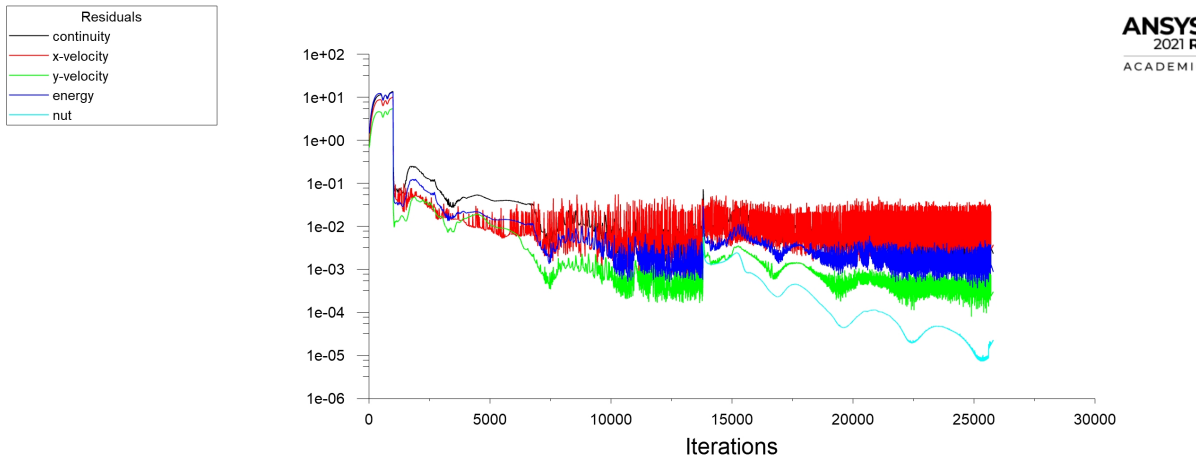


Figure 30 – Residuals for the Viscous simulation (14000 iterations)

Next chapter will discuss the results obtained.

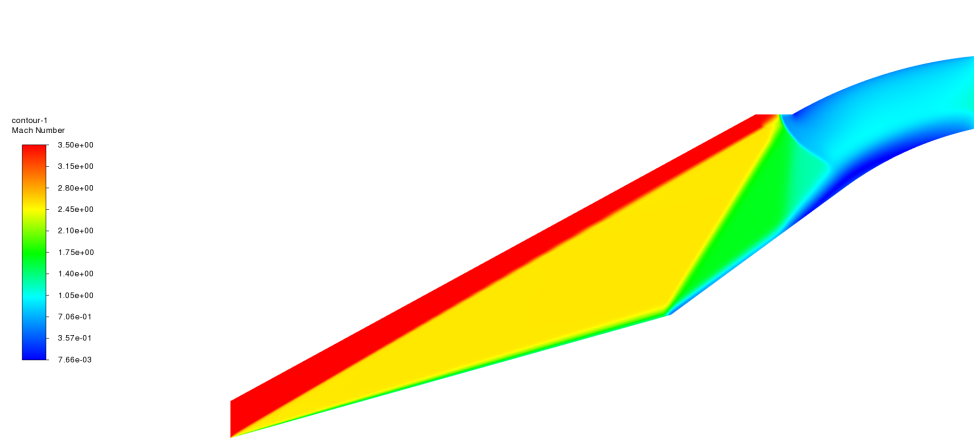
ANSYS
2021 R1
ACADEMIC

Figure 31 – Mach Number Field for the Viscous Flow

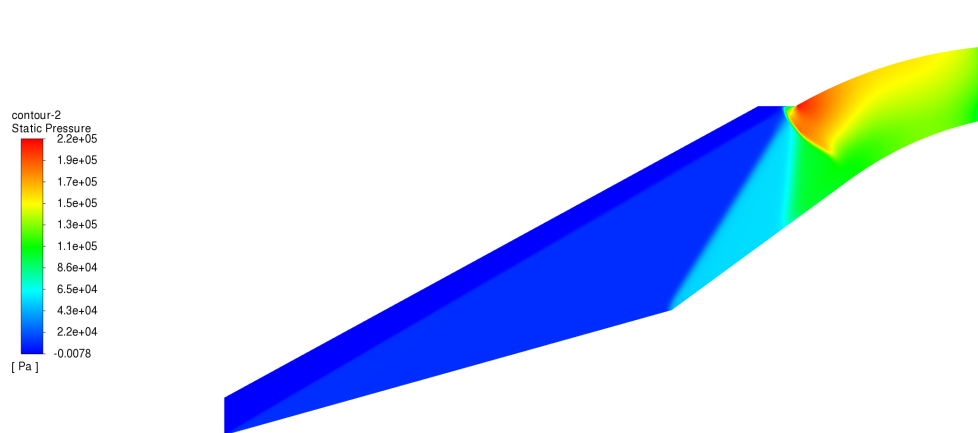
ANSYS
2021 R1
ACADEMIC

Figure 32 – Pressure Field for the Viscous Flow

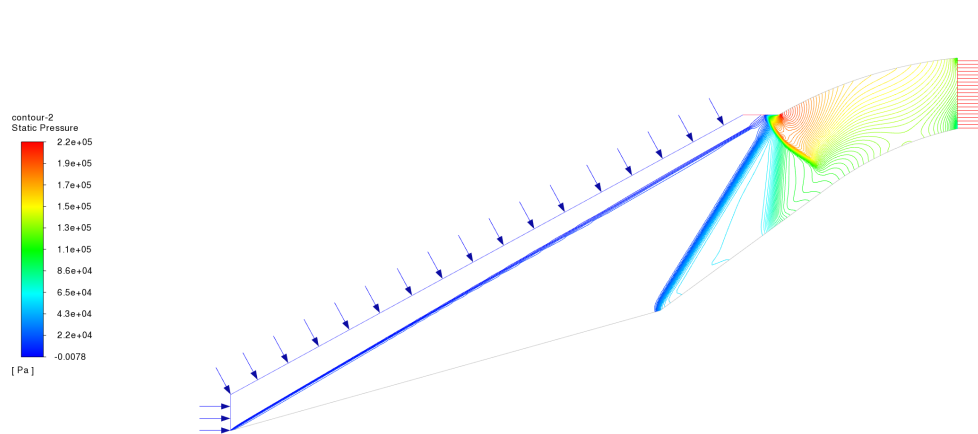
ANSYS
2021 R1
ACADEMIC

Figure 33 – Pressure Contour for the Viscous Flow

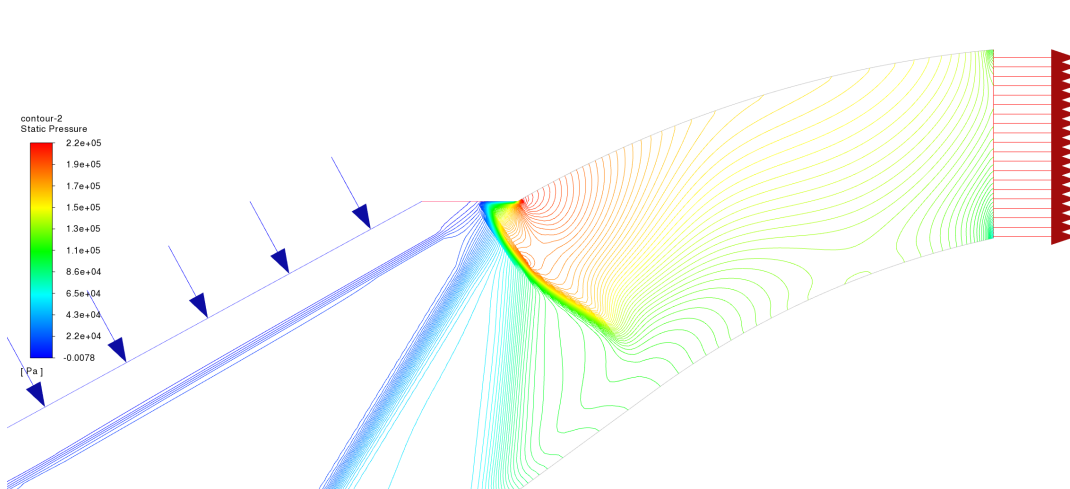


Figure 34 – Local Pressure contours for the Viscous Flow

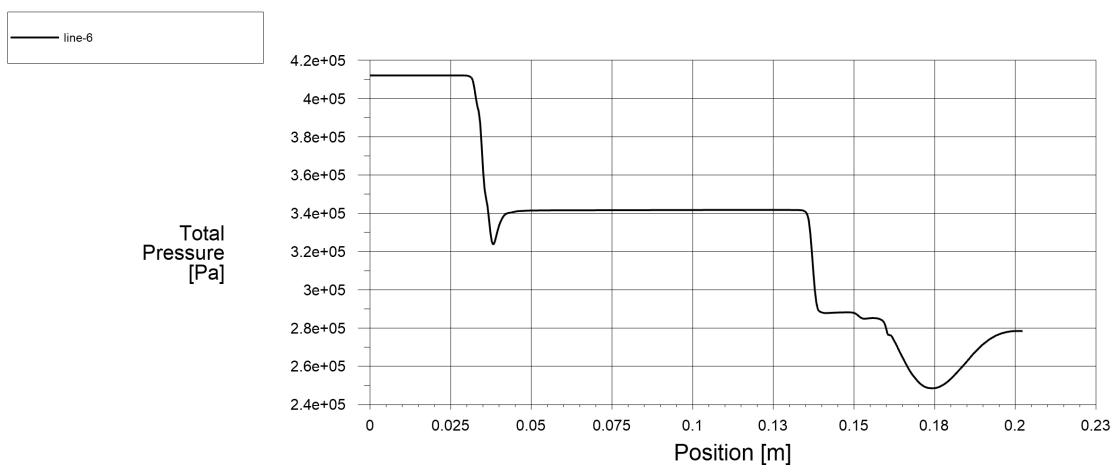


Figure 35 – Total Pressure Plot for the Viscous Flow

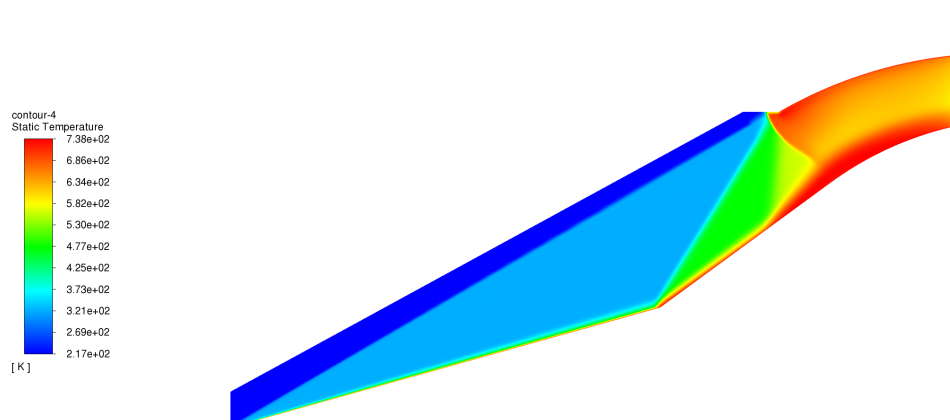


Figure 36 – Temperature Field for the Viscous Flow

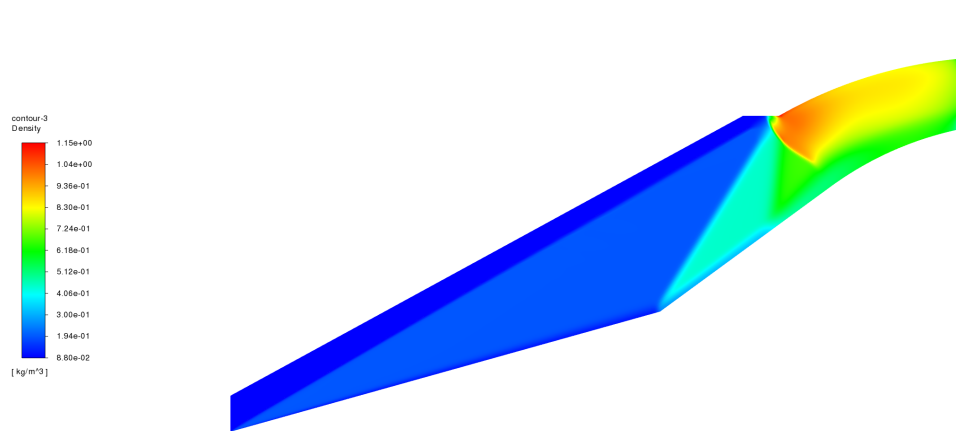
ANSYS
2021 R1
ACADEMIC

Figure 37 – Density Field for the Viscous Flow

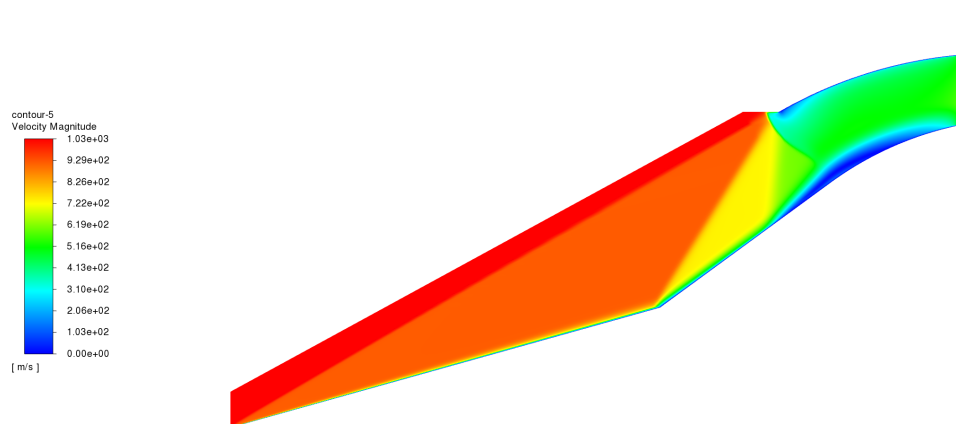
ANSYS
2021 R1
ACADEMIC

Figure 38 – Velocity Field for the Viscous Flow

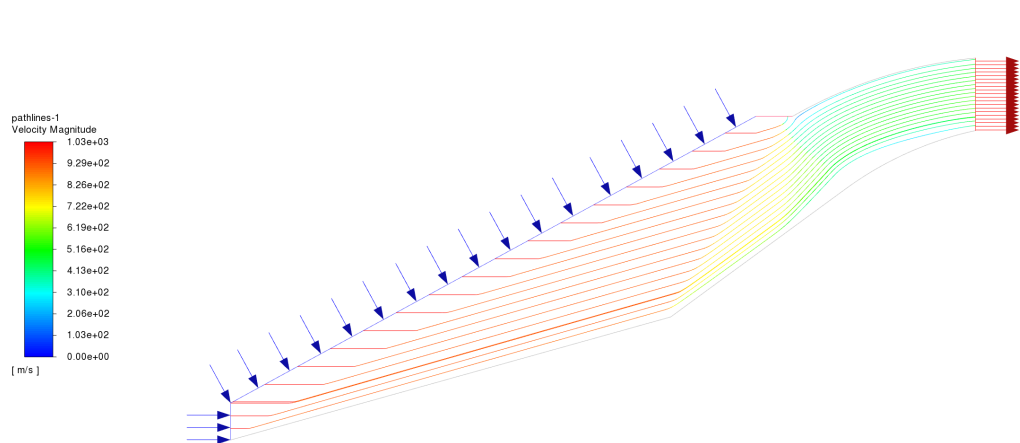
ANSYS
2021 R1
ACADEMIC

Figure 39 – Velocity Path-lines for the Viscous Flow

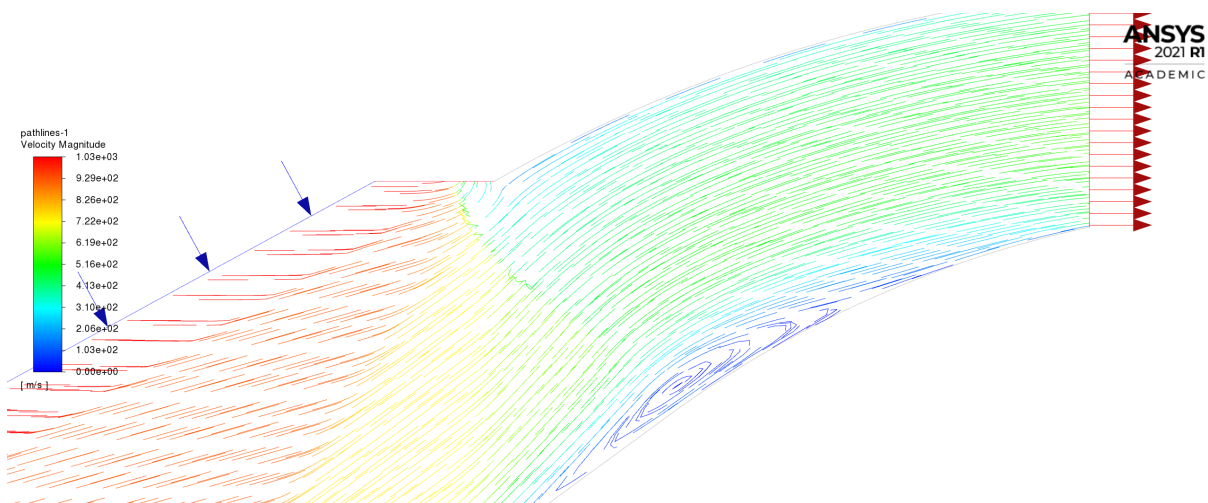


Figure 40 – Local Velocity Path-lines for the Viscous Flow

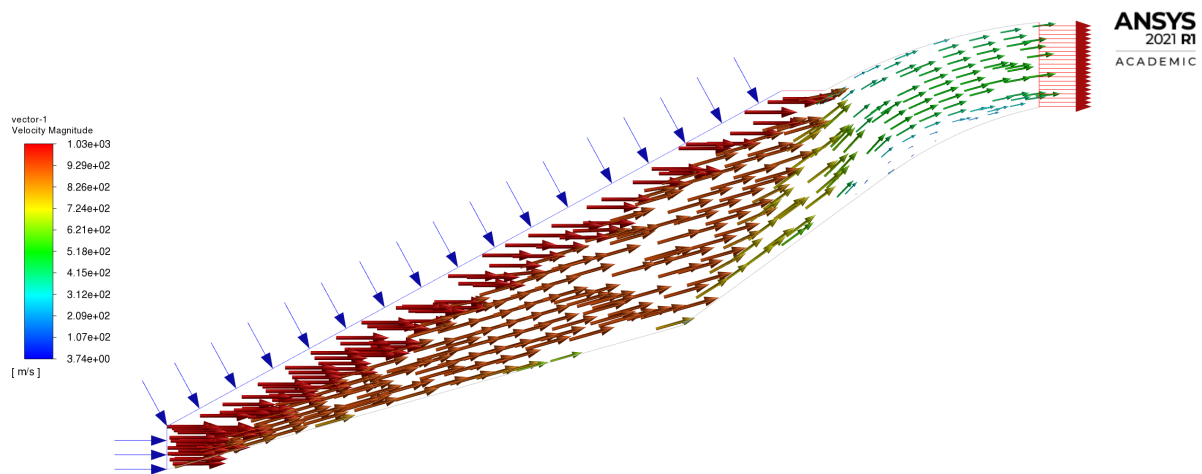


Figure 41 – Velocity Vectors for the Viscous Flow

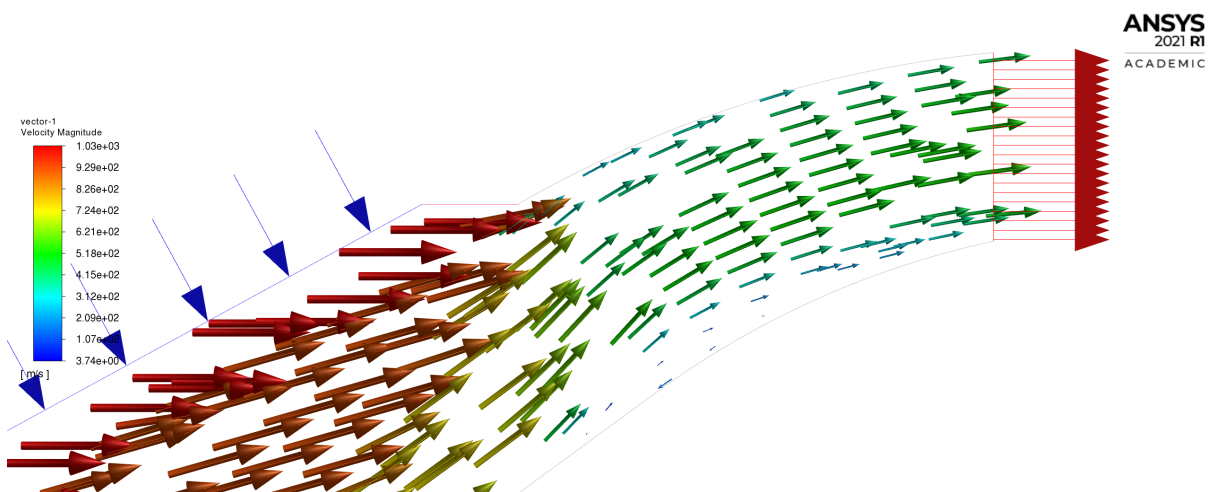


Figure 42 – Local Velocity Vectors for the Viscous Flow

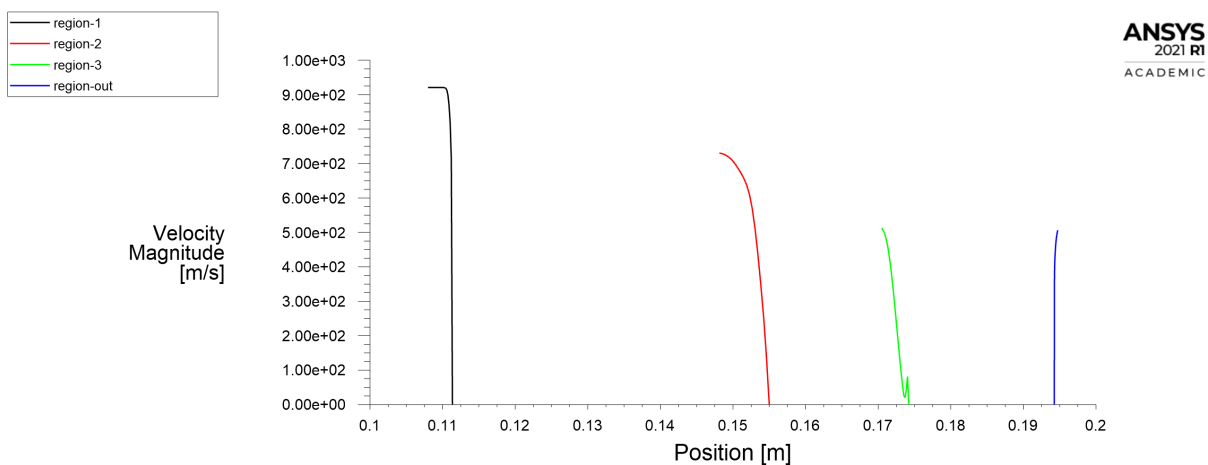


Figure 43 – Boundary Layer Detection

7 Discussion of Results of Part I

All the properties discussed in (TORRES, 2021) for Part I will be compared in the following sections.

The results presented in Figures 22 to 43 show us the expected behavior calculated analytically. From the perspective of numerical results, Tables 3 to 7 will help us with the comparison.

Mach Number

Parameter Station	Theoretical	Inviscid	$\varepsilon_{Inviscid} \%$	Viscous	$\varepsilon_{Viscous} \%$
0 (∞)	3.5	3.4988	0.0371	3.4987	0.0371
1	2.55	2.5693826	0.0751	2.4914	2.3499
2	1.65	1.6642	0.8606	1.5918	3.5273
3	0.66	0.6339	4.35	0.6236	5.52

Table 3 – Results of Mach Number for each station and errors

Pressure

Parameter Station	Theoretical	Inviscid	$\varepsilon_{Inviscid} \%$	Viscous	$\varepsilon_{Viscous} \%$
0 (∞)	5475	5475.001	1.8×10^{-5}	5475.257	0.0047
1	18580	18408	0.9257	18781.85	1.0863
2	63020	62219	1.2710	65219.67	3.4904
3	189120	186179	1.5551	182278	3.6178

Table 4 – Results of static Pressure for each station and errors

Temperature

Parameter Station	Theoretical	Inviscid	$\varepsilon_{Inviscid} \%$	Viscous	$\varepsilon_{Viscous} \%$
0 (∞)	216.65	216.6450	1.8×10^{-5}	216.6554	0.0025
1	325.82	321.8560	1.2166	334.4905	2.6611
2	489.97	480.3486	1.9637	503.8070	2.82
3	701.21	693.8642	1.0481	664.0875	5.2941

Table 5 – Results of Temperature for each station and errors

Density

Parameter Station	Theoretical	Inviscid	$\varepsilon_{Inviscid}$ %	Viscous	$\varepsilon_{Viscous}$ %
0 (∞)	0.088	0.0880	0.0449	0.0880	0.0475
1	0.20	0.1993	0.3500	0.1971	1.4300
2	0.45	0.4513	0.2889	0.4704	4.5333
3	0.94	0.9350	0.5319	0.9025	3.9900

Table 6 – Results of Density for each station and errors

Velocity

Parameter Station	Theoretical	Inviscid	$\varepsilon_{Inviscid}$ %	Viscous	$\varepsilon_{Viscous}$ %
0 (∞)	1030	1032	0.1941	1031.9943	0.1936
1	930	923.7193	0.6753	908.4665	2.3154
2	730	730.9041	0.1239	704.4702	3.4972
3	350	333.4146	4.7387	365.3221	4.3778

Table 7 – Results of Velocity for each station and errors

The expected shock wave behavior was obtained in all field graphs, and the errors were lower than 6%, making the simulation acceptable. With respect to the residuals, there still some margin to convergence, but 1.6% margin is sufficient, since the normal shock is the reason why analytical calculations did not match exactly the simulation for the inviscid flow. From the plot of Total pressure, we can easily identify the phenomena of the shock wave occurring in each station, representing a decrease in total pressure along the device.

Relative to the velocity pathlines and vector field, the system had the expected result for the inviscid flow and viscous flow. Due to the presence of the boundary layer as can be visualized from the viscous fields, is the main reason why the perfect results were not obtained from the viscous model, and represent the boundary layer in the model, and the representation is contained in the velocity plot next to the walls (Figures 34, 40, 42 and 43).

Part II

Conical and Bell-Shaped Nozzles

8 Geometry Description

To complement the first part, where we developed a diffuser with optimal characteristics at the altitude of 22 km and Mach Number 3.5, in this part, two different configurations of ramjet nozzles have their analytical results compared to their numerical simulation result. The figure 44 shows all the stations of the device and Figure 45 show both developed geometries in (TORRES, 2021).

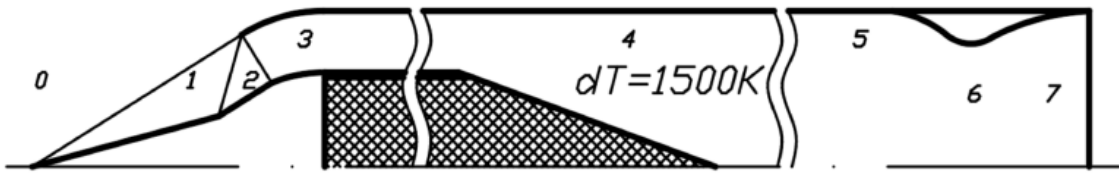


Figure 44 – RAMJET from work 1.

The two geometries for the nozzle are shown in Figures 46 and 47. The same procedure applied in the previous chapter will be followed. Table 8 show the analytical value for the entire geometry starting from station 3.

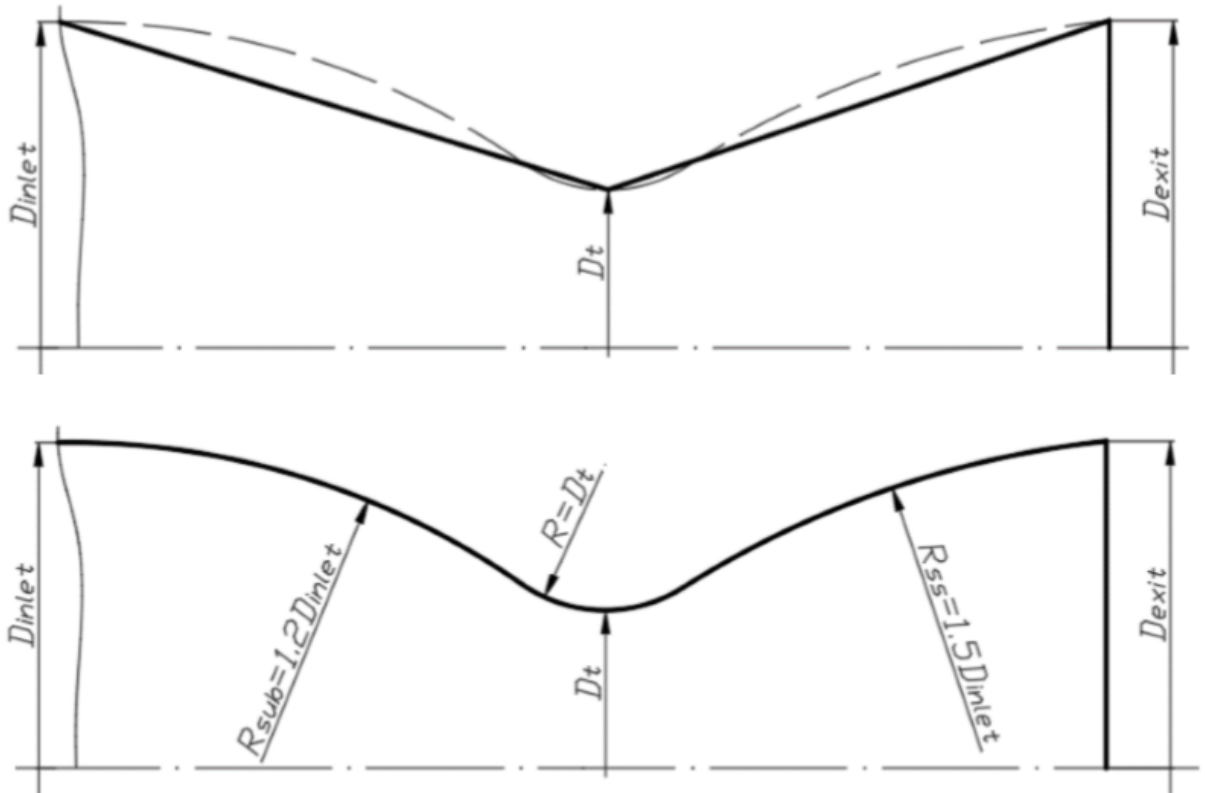


Figure 45 – Proposed nozzle designs in work 1.

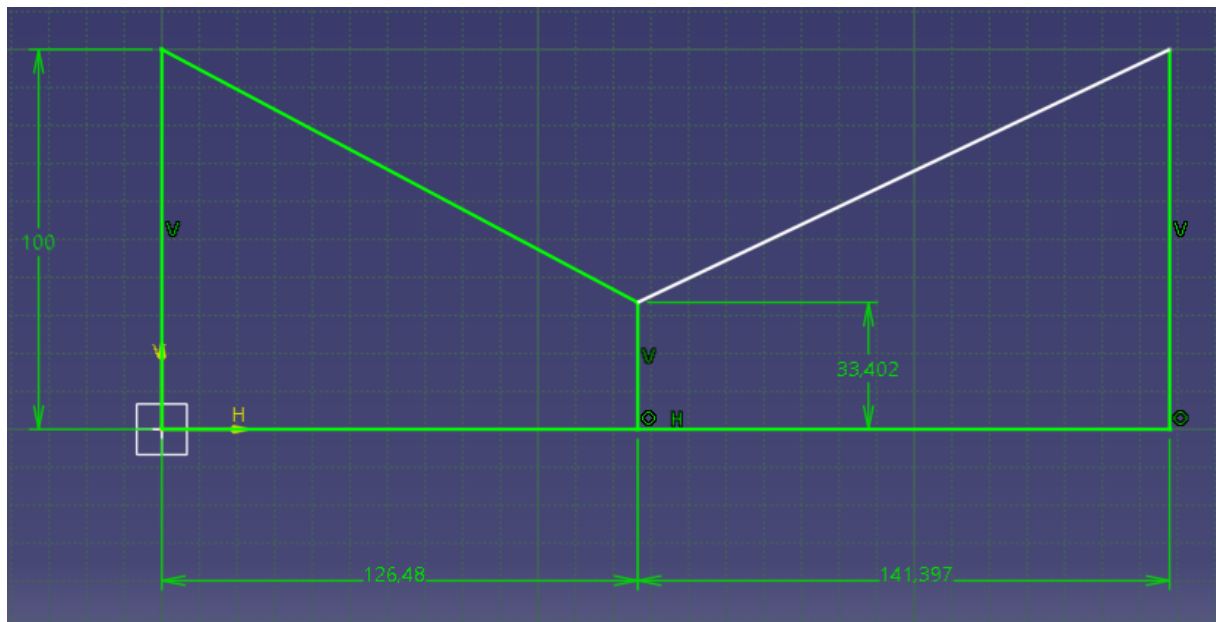


Figure 46 – Conical Geometry. Source: (TORRES, 2021)

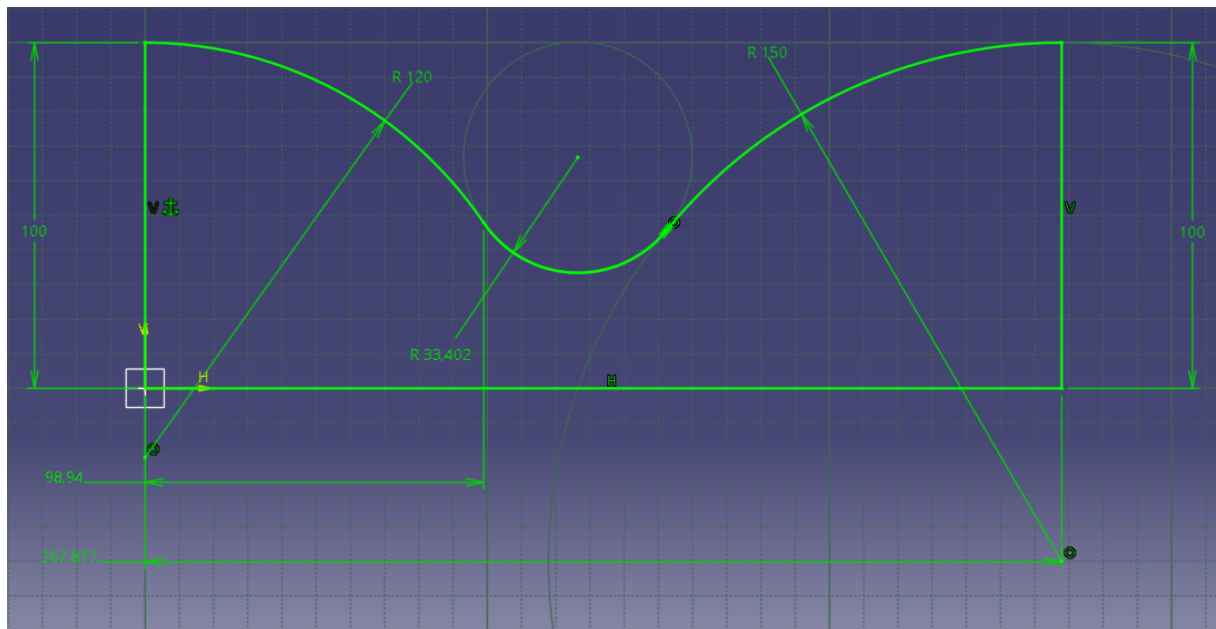


Figure 47 – Bell-Shaped Geometry. Source: (TORRES, 2021)

Parameter \ Station	3	4	5	6	7
Mach Number	0.66	0.13	0.20	1.00	2.65
Static Pressure [kPa]	189115.27	250239.60	242466.60	131154.41	11603.08
Temperature [K]	701.21	760.92	1760.92	1519.05	748.59
Velocity [km/s]	349.78	69.90	166.95	784.60	1459.85
Density [kg/m³]	0.94	1.15	0.48	0.31	0.06

Table 8 – Design Parameters for each Station at second part. Source: (TORRES, 2021)

9 Nozzle Setup

The procedures adopted here follow the same strategy approached in chapter 4. Since the design process in the nozzles have all constraints already established, the mesh was based in the original design done in ([TORRES, 2021](#)).

9.1 Mesh Settings

The meshes created for each geometry are shown from Figure 48 to 51, including the number of elements and nodes in the menu.

The division of sides here were based on the height of the inlet and outlet and similarly for the walls and symmetry region. The same principle of division per elements was made here, the only difference is that both geometries had a bias based on the flow behavior next to the walls.

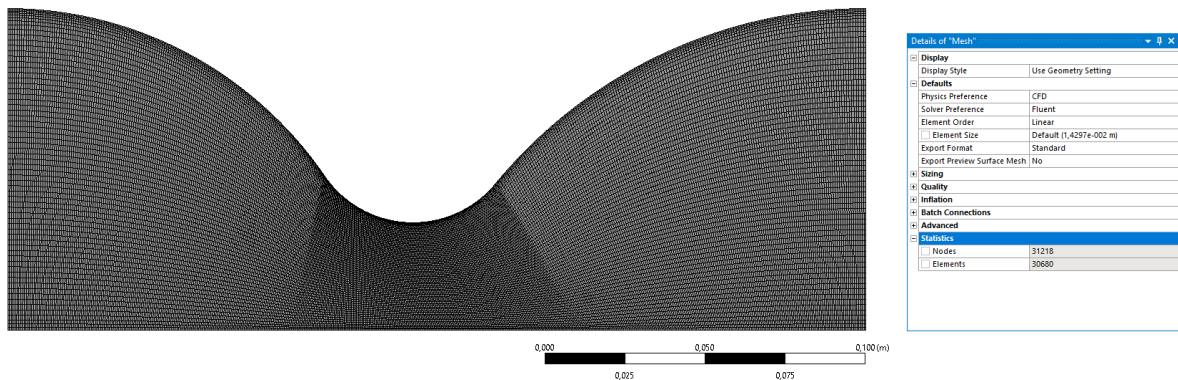


Figure 48 – Mesh for the Bell-Shaped Nozzle with inviscid flow.

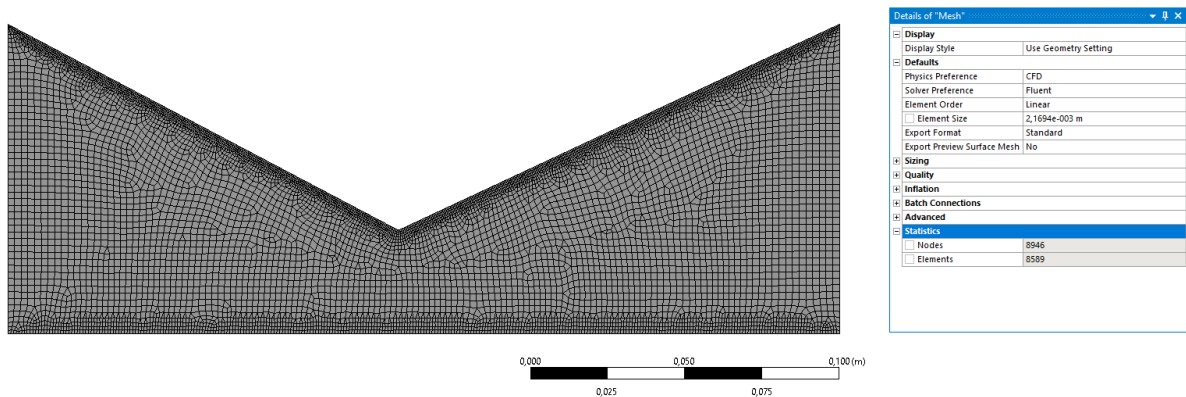


Figure 49 – Mesh for the Conical-Shaped Nozzle with inviscid flow.

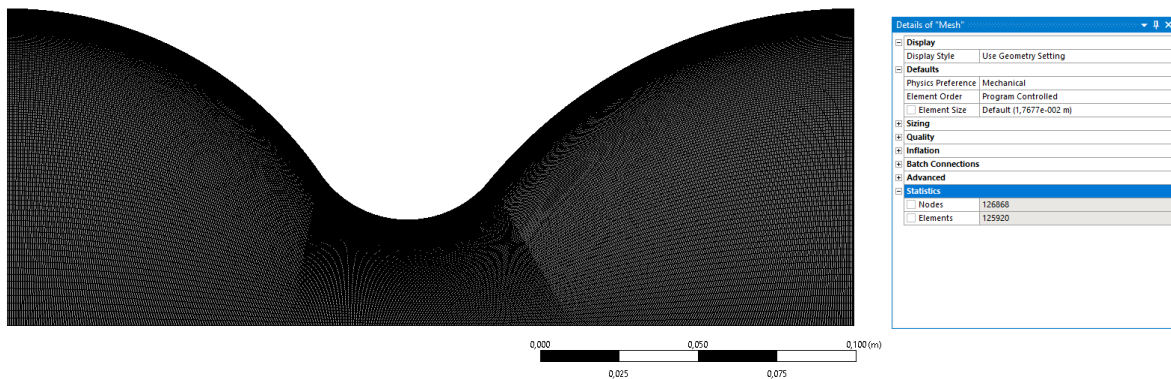


Figure 50 – Mesh for the Bell-Shaped Nozzle with viscous flow

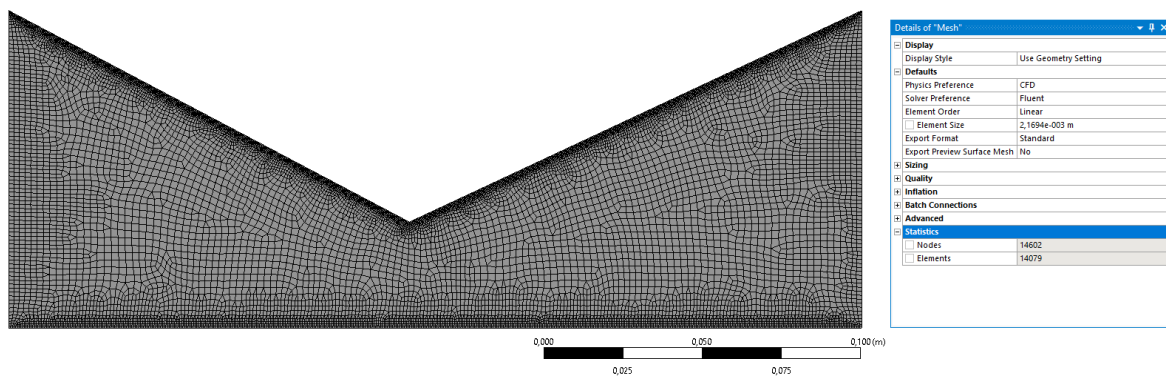


Figure 51 – Mesh for the Conical-Shaped Nozzle with viscous flow

9.2 Mesh Quality

As previously explained, the metrics used to determine the quality of the meshes were based on the Section 4.2. The results are illustrated in Figures 52 to 57.

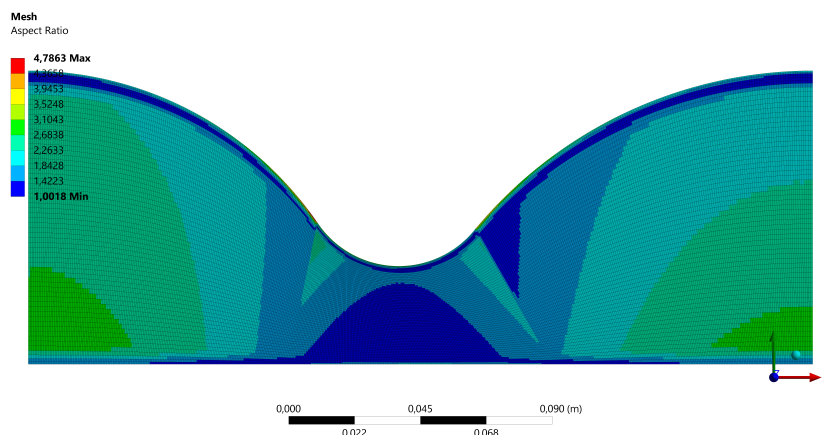


Figure 52 – Mesh quality for Aspect Ratio Metric for the Bell-Shaped geometry and inviscid flow.

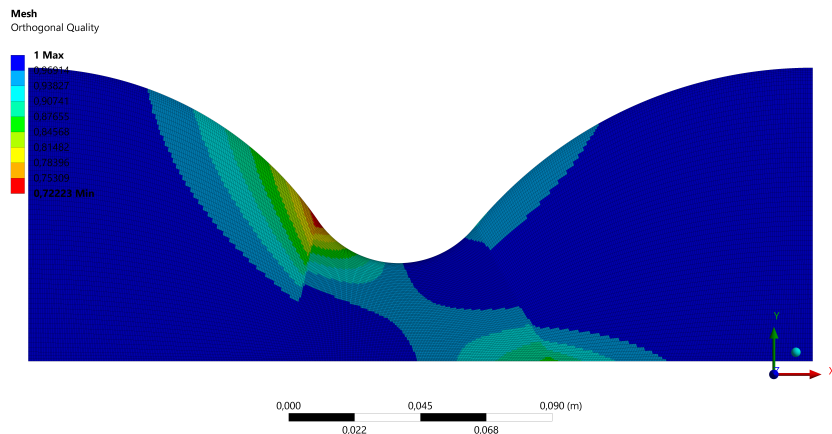


Figure 53 – Mesh quality for Orthogonality Metric for the Bell-Shaped geometry and inviscid flow.

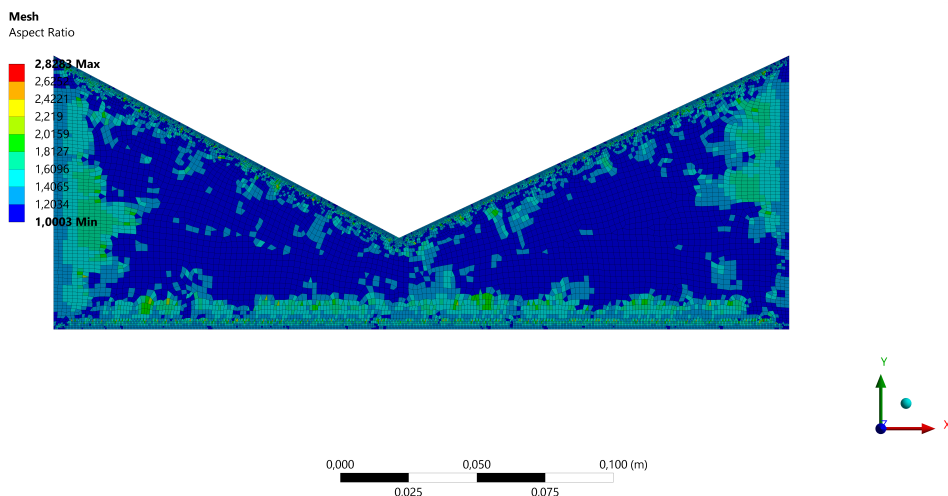


Figure 54 – Mesh quality for Aspect Ratio Metric for the Conical geometry and inviscid flow.

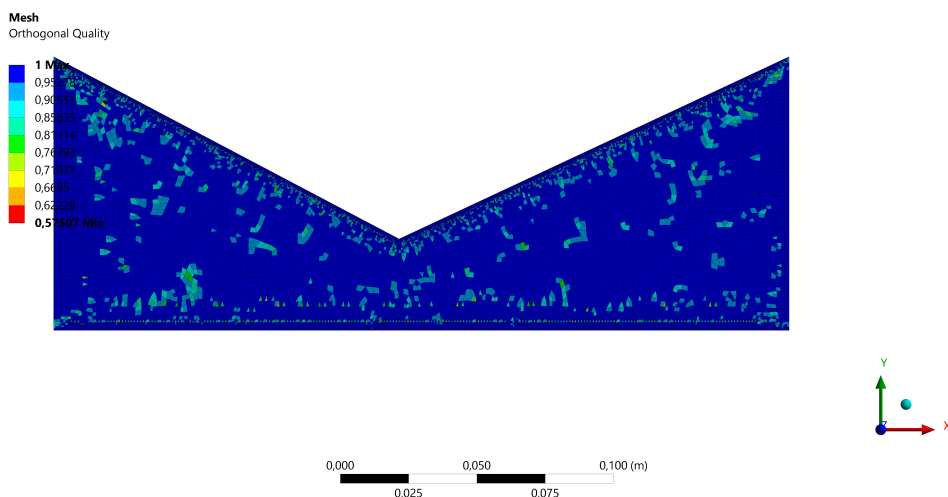


Figure 55 – Mesh quality for Orthogonality Metric for the Conical geometry and inviscid flow.

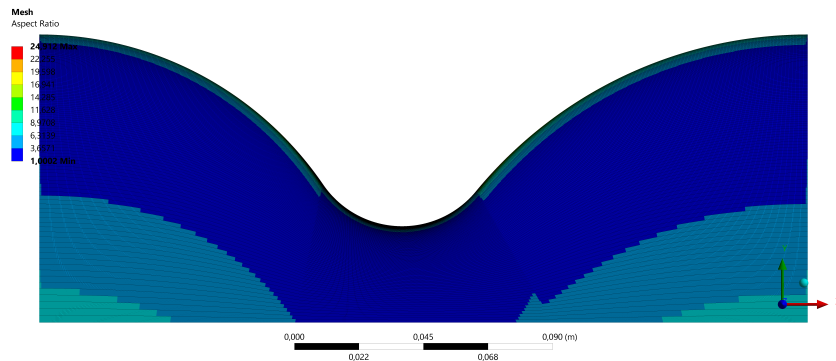


Figure 56 – Mesh quality for Aspect Ratio Metric for the Bell-Shaped geometry and viscous flow.

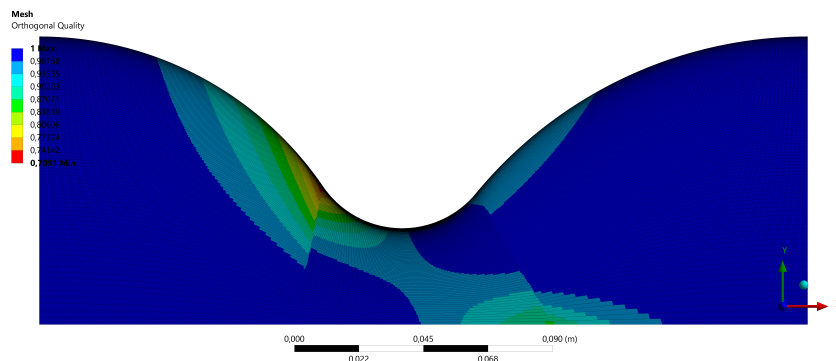


Figure 57 – Mesh quality for Orthogonality Metric for the Bell-Shaped geometry and viscous flow.

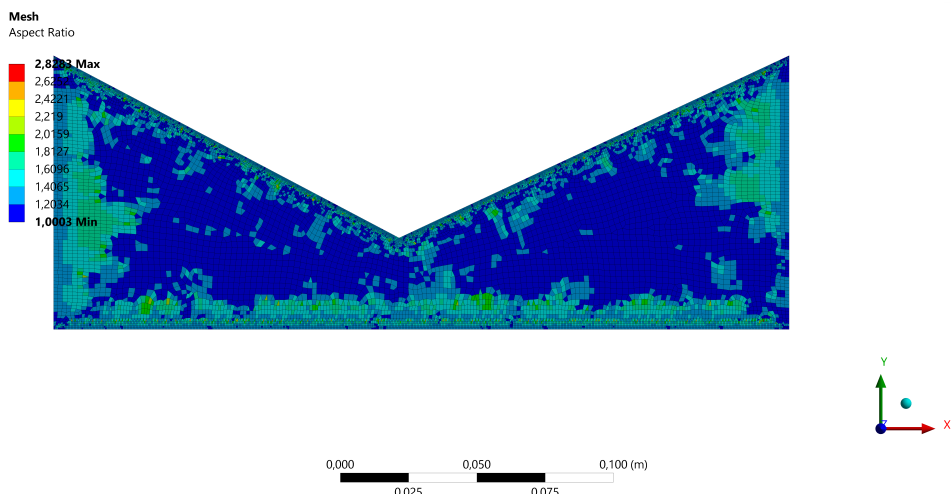


Figure 58 – Mesh quality for Aspect Ratio Metric for the Conical geometry and Viscous flow.

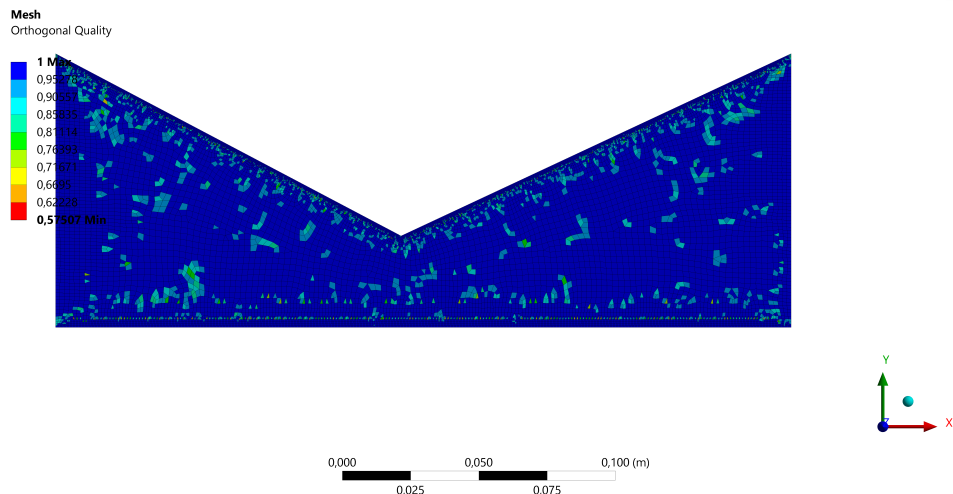


Figure 59 – Mesh quality for Orthogonality Metric for the Conical geometry and Viscous flow.

9.3 Fluent Setup

From the panel on ANSYS Fluent (Figure 60), the following set of configurations was modified:

Setup -> General: From *Pressure Based* to *Density Based*;

Setup -> Models: *Energy* (On) / *Viscous* (Inviscid);

Setup -> Materials -> Fluid -> air : *Density* (ideal-gas);

To clarify the boundary conditions, Figure 61 will serve as a reference.

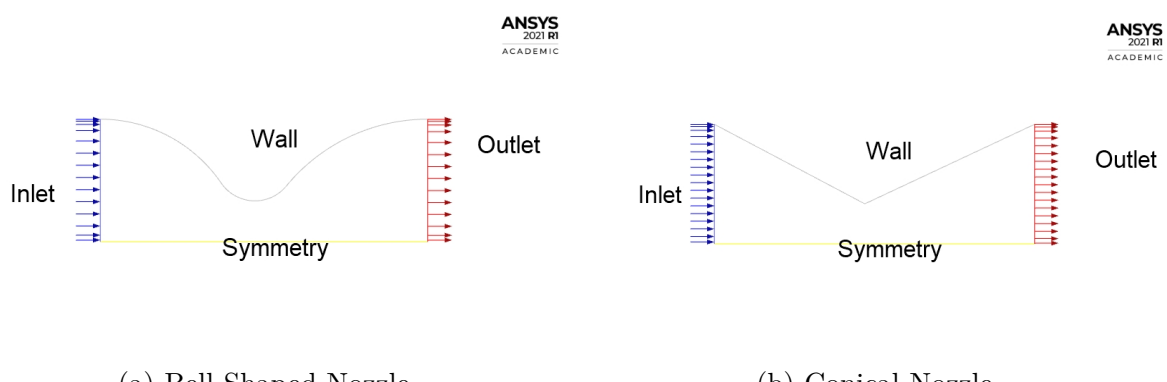


Figure 61 – Boundary Conditions: Nozzle.

Setup -> Boundary Conditions -> Inlet : Figure 62 contains the settings; change the condition type to *Pressure Inlet*;

Setup -> Boundary Conditions -> Outlet : Figure 63 contains the settings, change the condition type to *Pressure Outlet*:

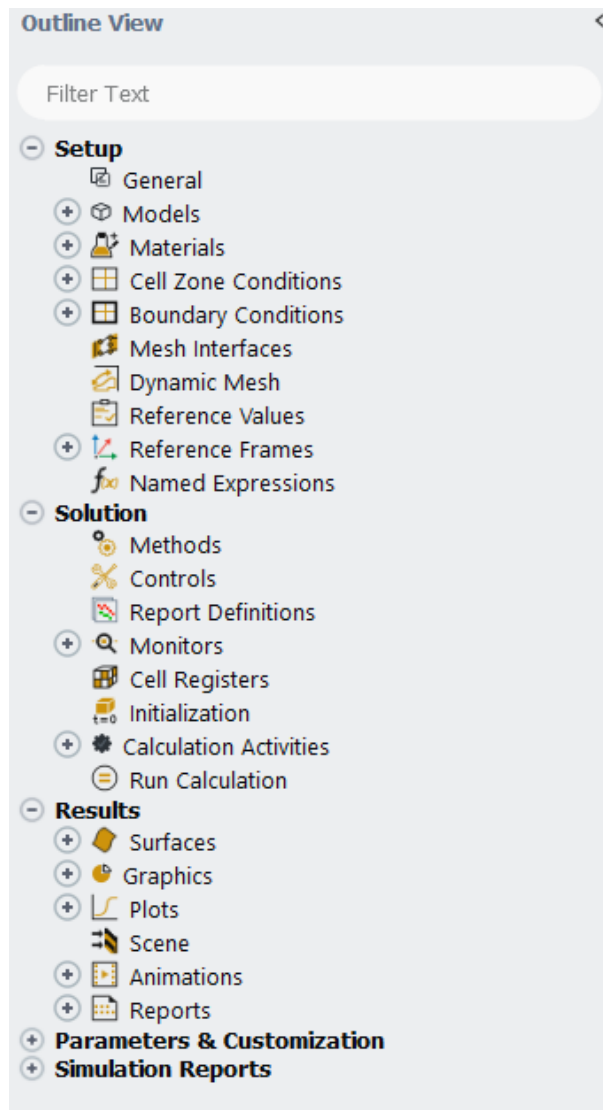
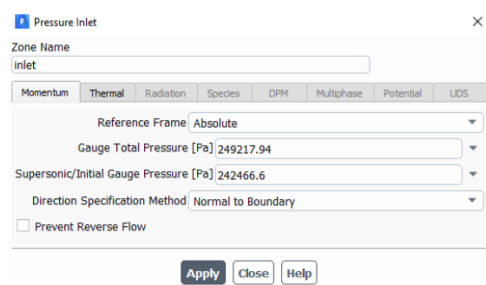


Figure 60 – Ansys Fluent Panel



(a) Momentum window



(b) Thermal window

Figure 62 – Boundary Conditions: Inlet

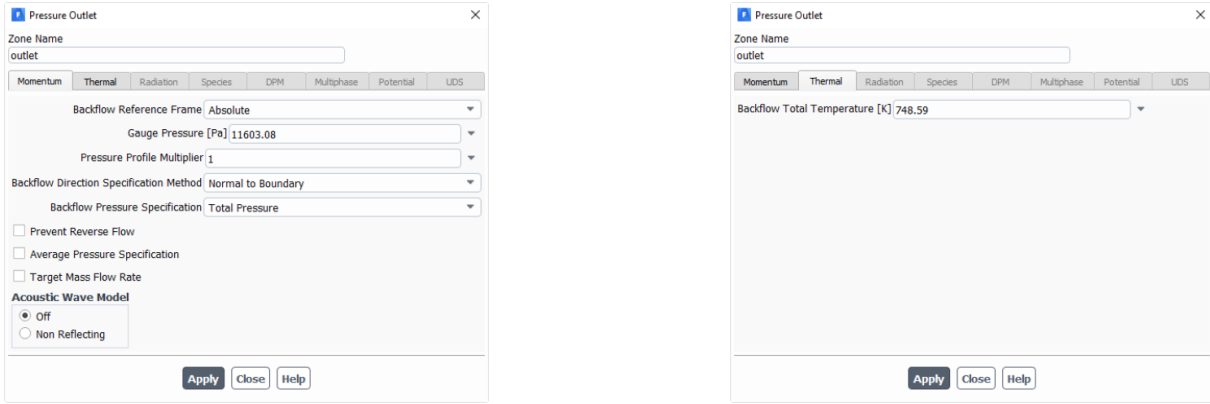


Figure 63 – Boundary Conditions: Outlet

Solution -> Methods : *Flow* (First Order Upwind), this option was chosen to the simulation due to its stability and lower processing time. Inside the panel, in *High Order Term Relaxation* the *Relaxation Factor* was set 0.5 and the option *Variables* was changed to *all variables*;

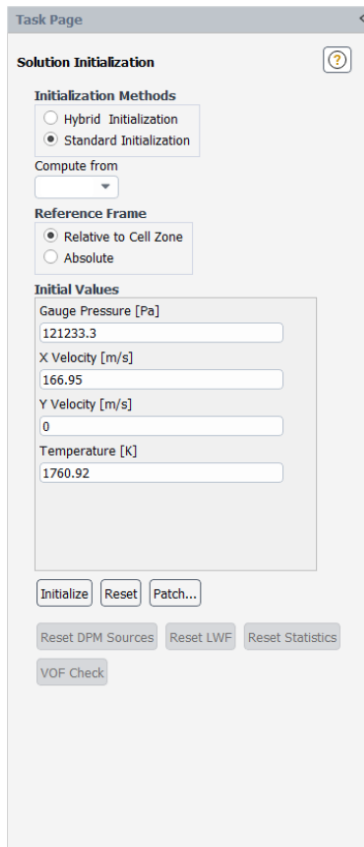
Solution -> Controls : *Courant Number* 3.

Solution -> Initialization : Figure 64a contains the settings. Attention for the *Gauge Pressure* in the initialization (half the value at the inlet).

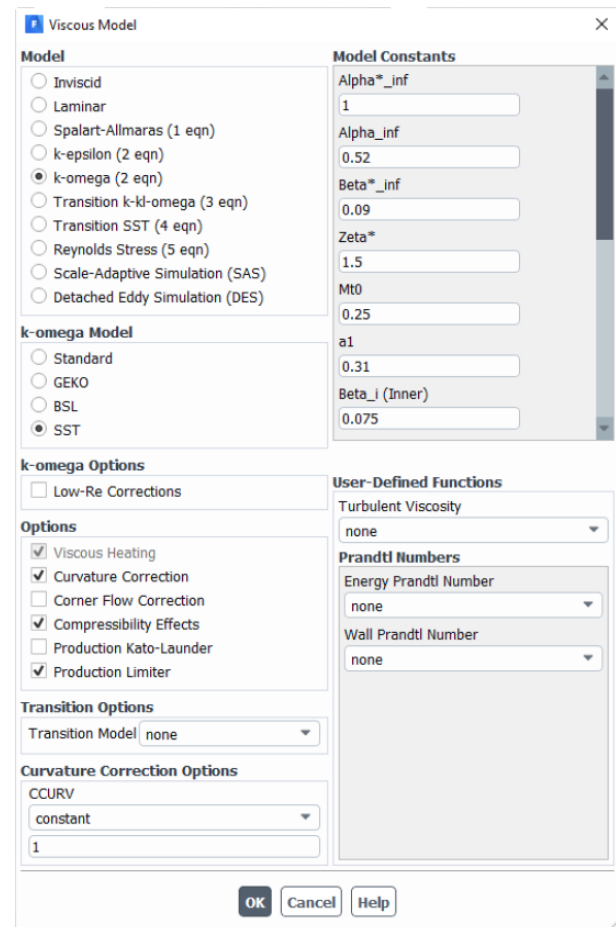
9.3.1 Viscous Flow modifications

Setup -> Models: *Energy* (On) / *Viscous* (k-omega 2 eqn). The configurations are presented in Figure 64b.

Some procedures as animating the solution and interpolating the data from the inviscid simulation to the viscous simulation can improve the processing time. The methods utilized in chapter 5 can be applied to obtain the results of the next chapter.



(a) Initialization window



(b) k-omega Configurations.

Figure 64 – Boundary Conditions: Outlet

10 Results of Part II

All results obtained for both geometries will be organized according to their shape/flow. Figures 65 to 80 refers to the Bell-Shaped nozzle and Figures 81 to 96. If necessary zoom in for better details in the graphs.

10.1 Bell-Shaped Nozzle

10.1.1 Inviscid Part

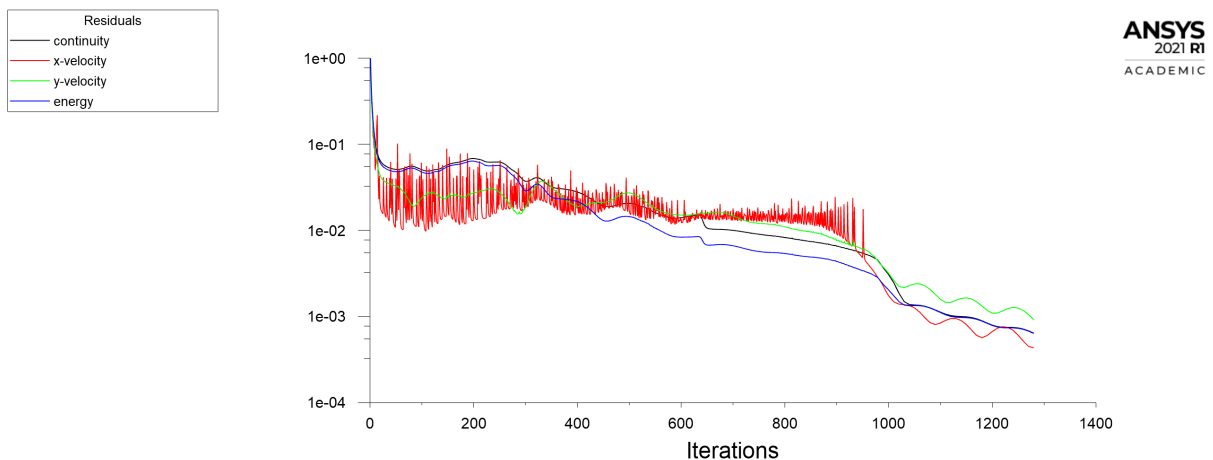


Figure 65 – Residuals for the inviscid simulation of the Bell-Shaped Nozzle

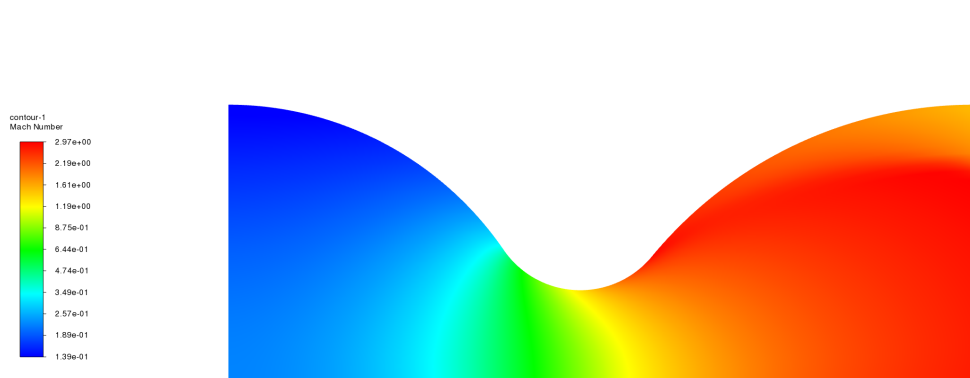
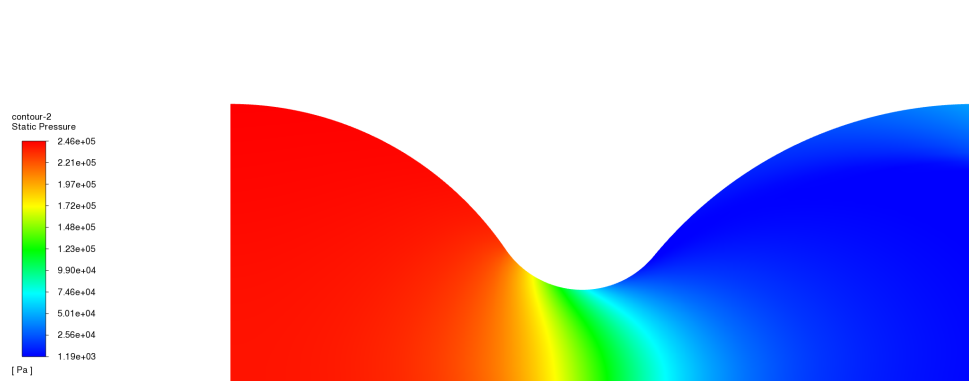
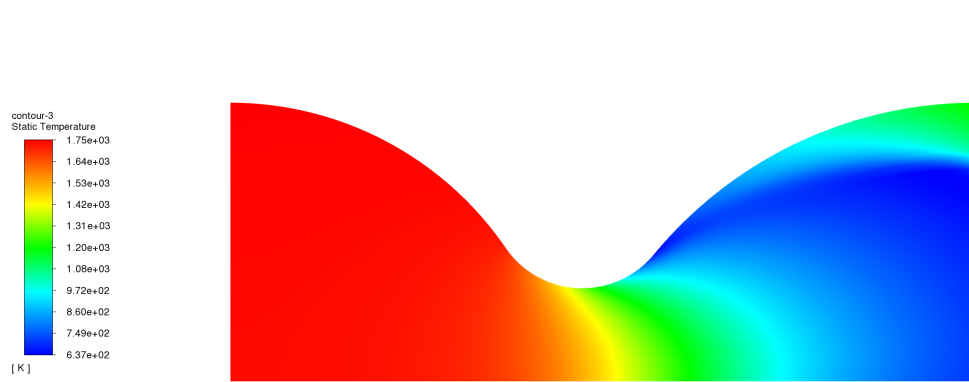


Figure 66 – Mach Number Field for the inviscid simulation of the Bell-Shaped Nozzle



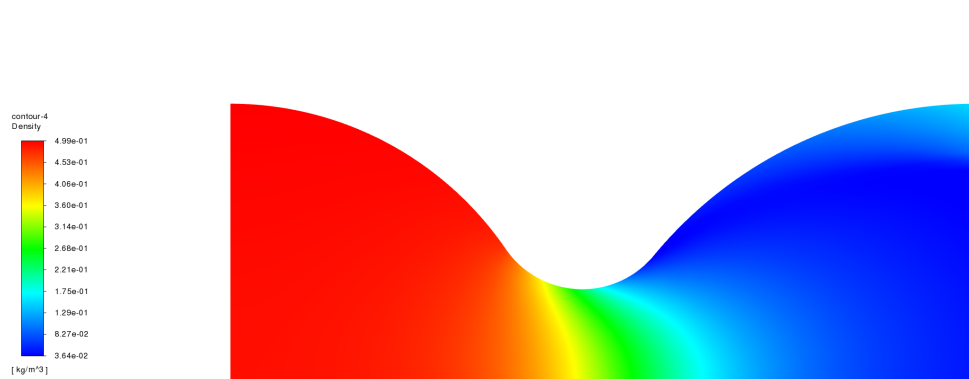
ANSYS
2021 R1
ACADEMIC

Figure 67 – Pressure Field for the inviscid simulation of the Bell-Shaped Nozzle



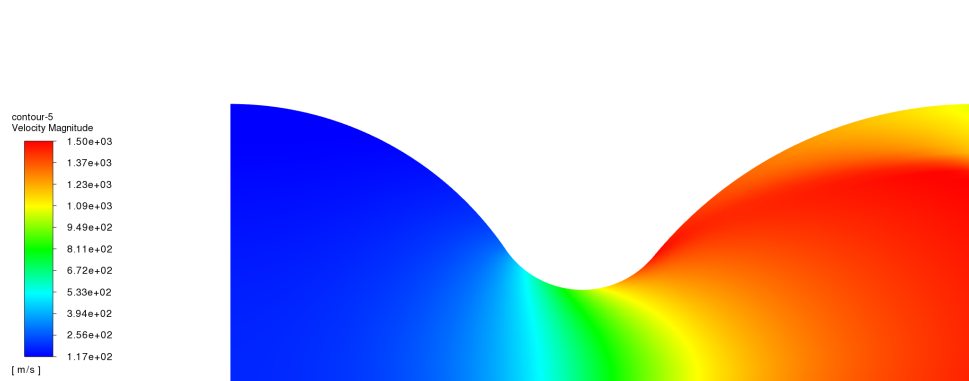
ANSYS
2021 R1
ACADEMIC

Figure 68 – Temperature Field for the inviscid simulation of the Bell-Shaped Nozzle



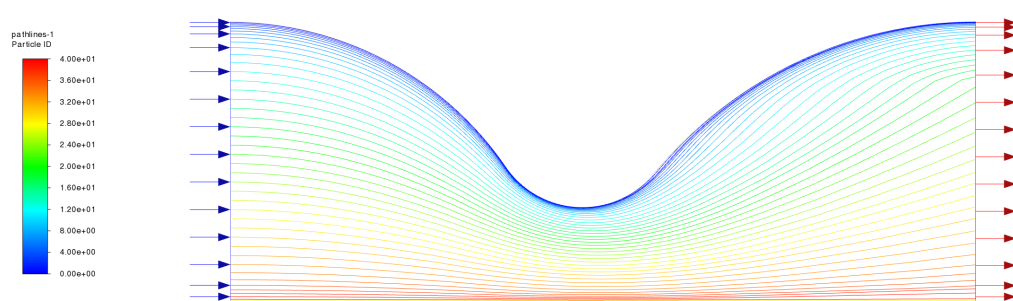
ANSYS
2021 R1
ACADEMIC

Figure 69 – Density Field for the inviscid simulation of the Bell-Shaped Nozzle



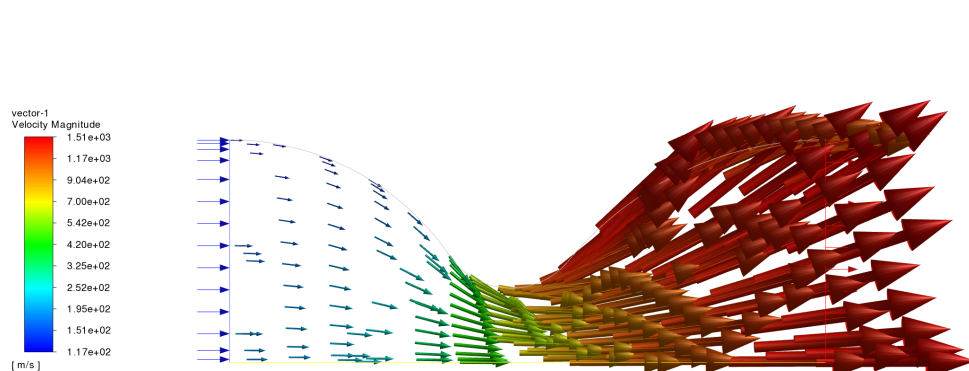
ANSYS
2021 R1
ACADEMIC

Figure 70 – Velocity Field for the inviscid simulation of the Bell-Shaped Nozzle



ANSYS
2021 R1
ACADEMIC

Figure 71 – Velocity Path-lines for the inviscid simulation of the Bell-Shaped Nozzle



ANSYS
2021 R1
ACADEMIC

Figure 72 – Velocity Vector Field for the inviscid simulation of the Bell-Shaped Nozzle

10.1.2 Viscous

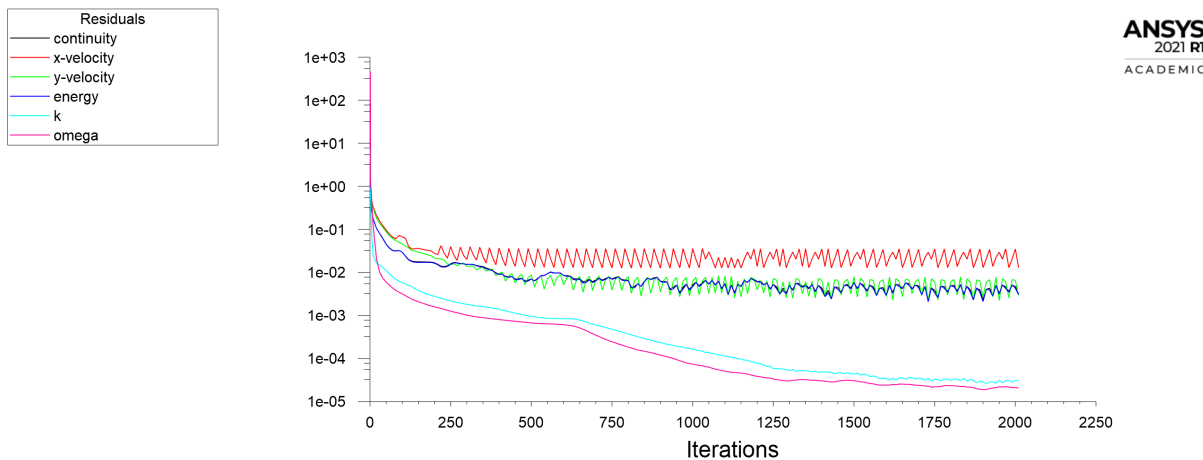


Figure 73 – Residuals for the Viscous simulation of the Bell-Shaped Nozzle

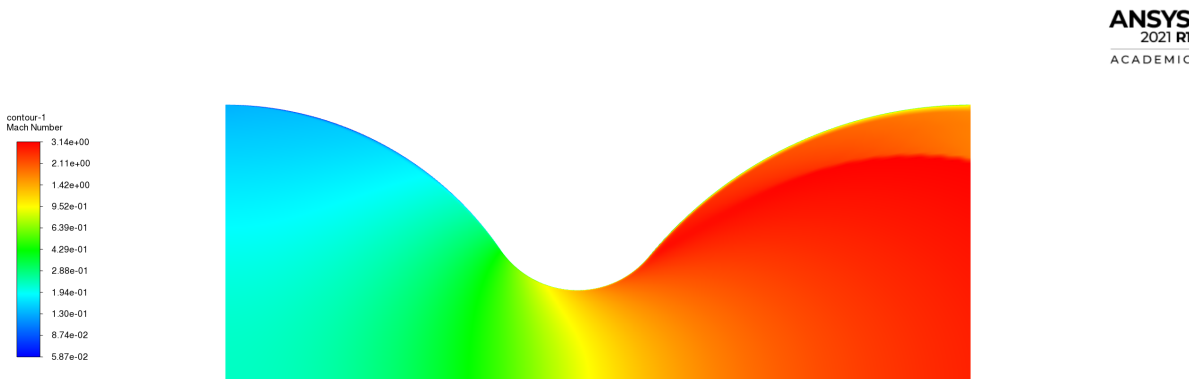


Figure 74 – Mach Number Field for the Viscous simulation of the Bell-Shaped Nozzle

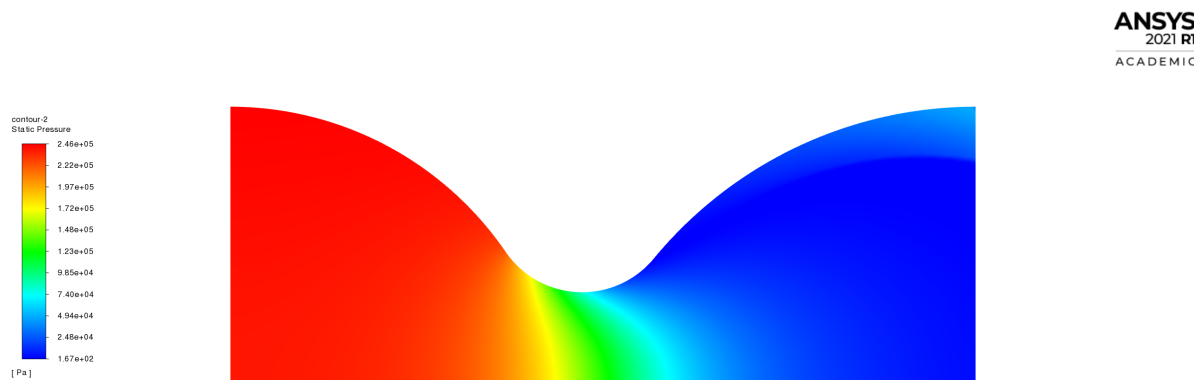


Figure 75 – Pressure Field for the Viscous simulation of the Bell-Shaped Nozzle

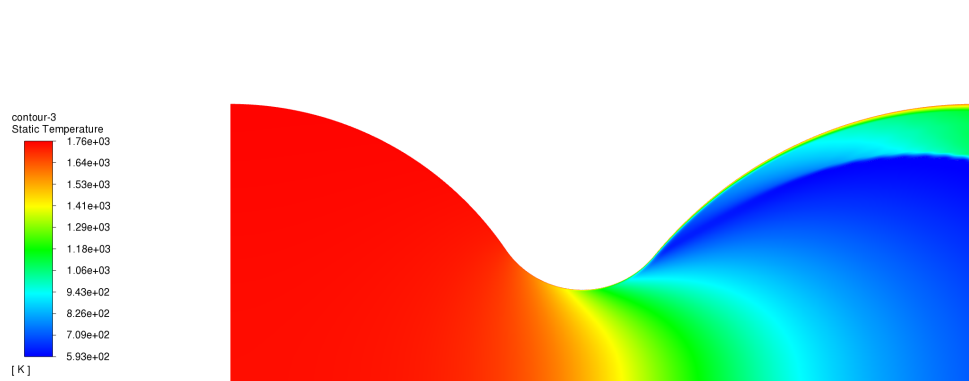


Figure 76 – Temperature Field for the Viscous simulation of the Bell-Shaped Nozzle

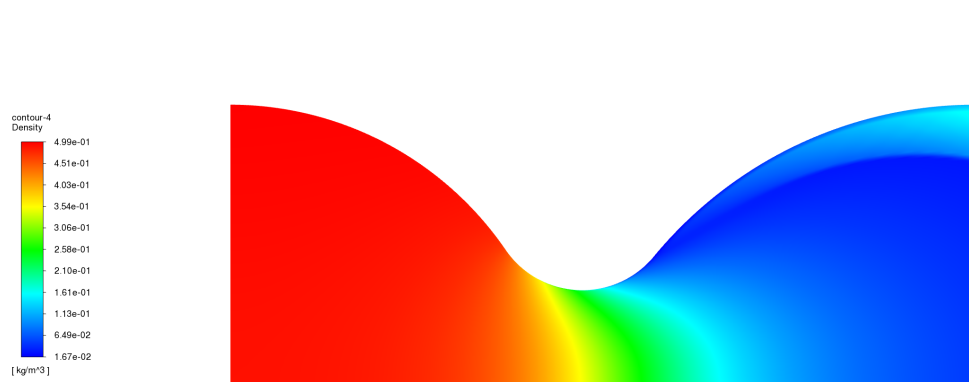


Figure 77 – Density Field for the Viscous simulation of the Bell-Shaped Nozzle

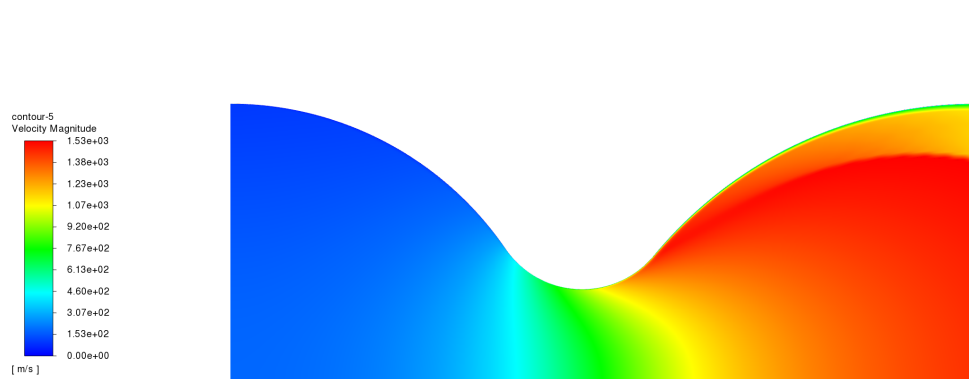


Figure 78 – Velocity Field for the Viscous simulation of the Bell-Shaped Nozzle

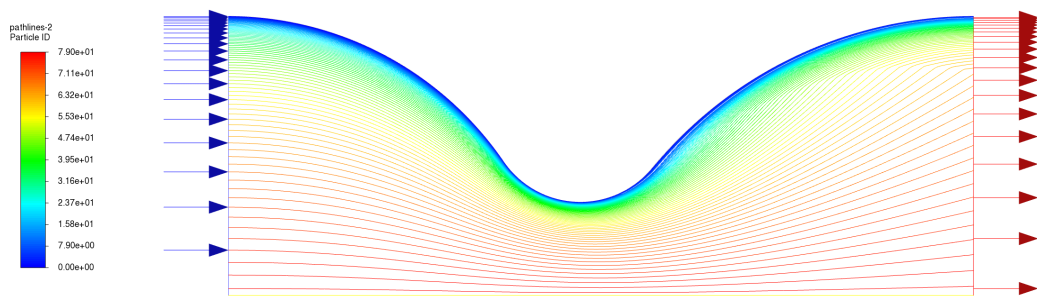


Figure 79 – Velocity Path-lines for the Viscous simulation of the Bell-Shaped Nozzle

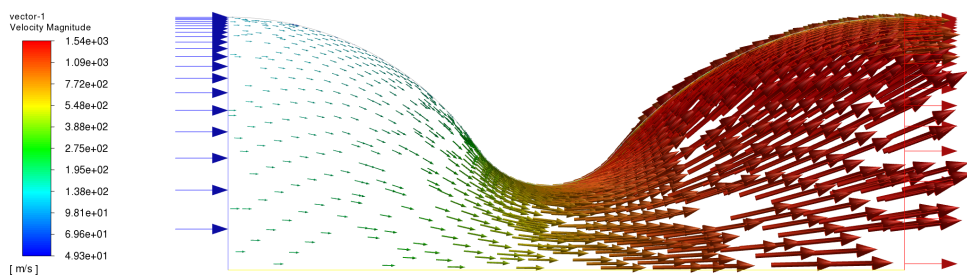


Figure 80 – Velocity Vector Field for the Viscous simulation of the Bell-Shaped Nozzle

10.2 Conical-Shaped Nozzle

10.2.1 Inviscid

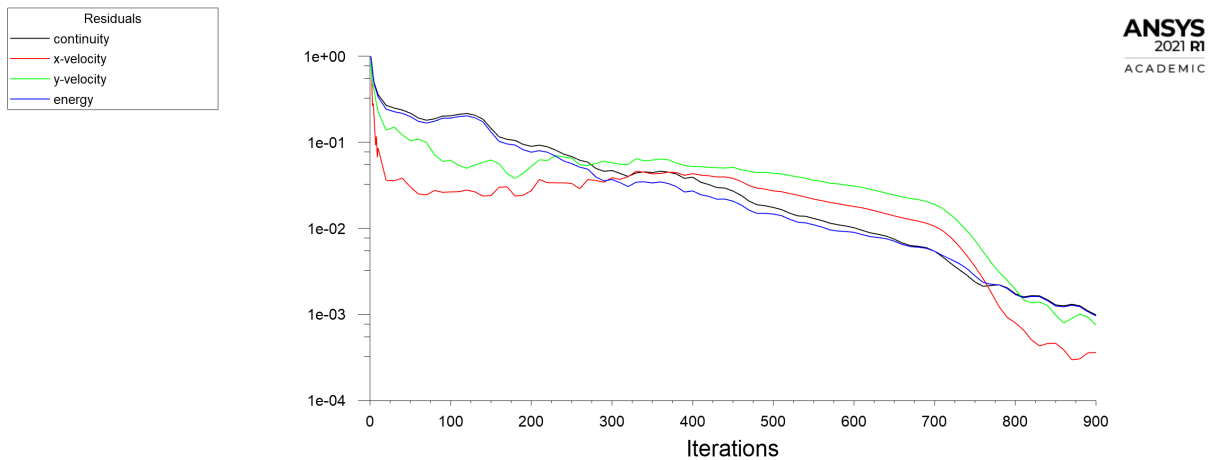


Figure 81 – Residuals for the inviscid simulation of the Conical-Shaped Nozzle

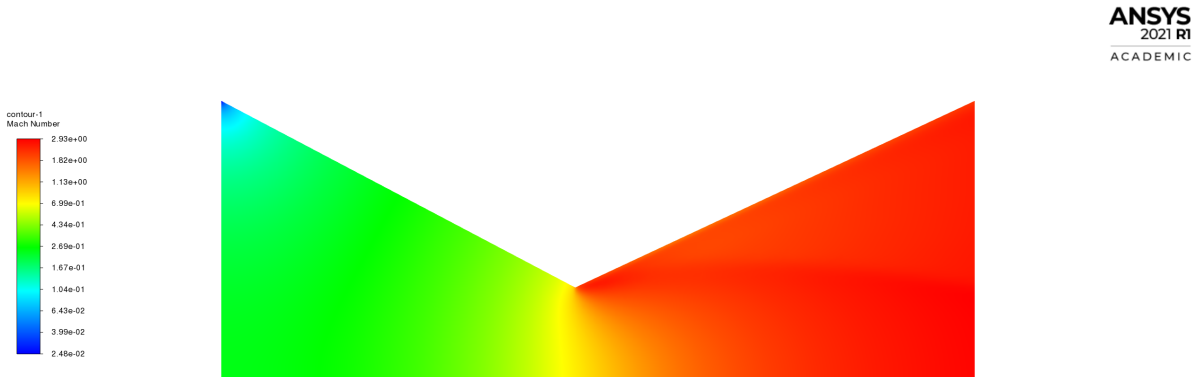


Figure 82 – Mach Number Field for the inviscid simulation of the Conical-Shaped Nozzle

ANSYS
2021 R1
ACADEMIC

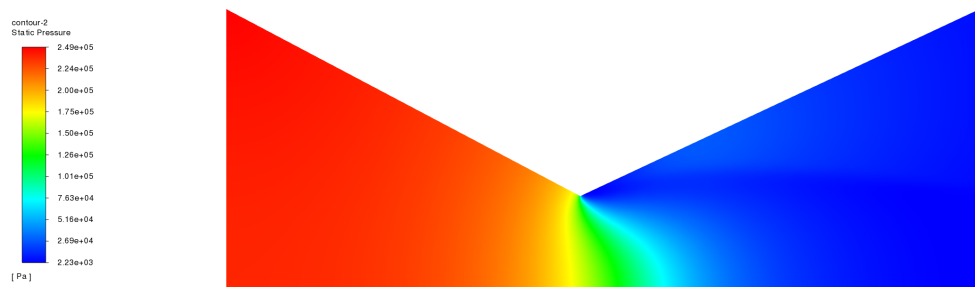


Figure 83 – Pressure Field for the inviscid simulation of the Conical-Shaped Nozzle

ANSYS
2021 R1
ACADEMIC

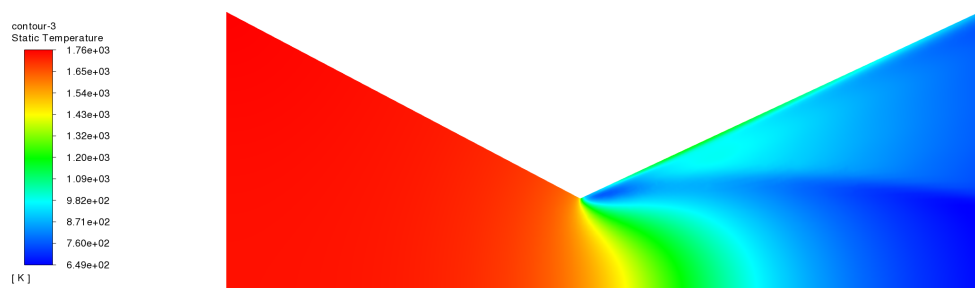


Figure 84 – Temperature Field for the inviscid simulation of the Conical-Shaped Nozzle

ANSYS
2021 R1
ACADEMIC

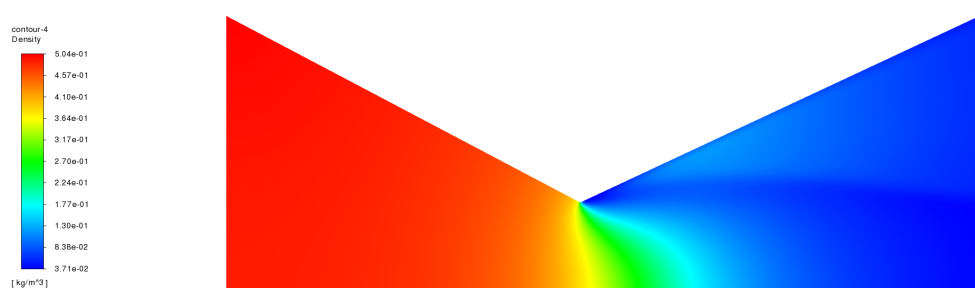
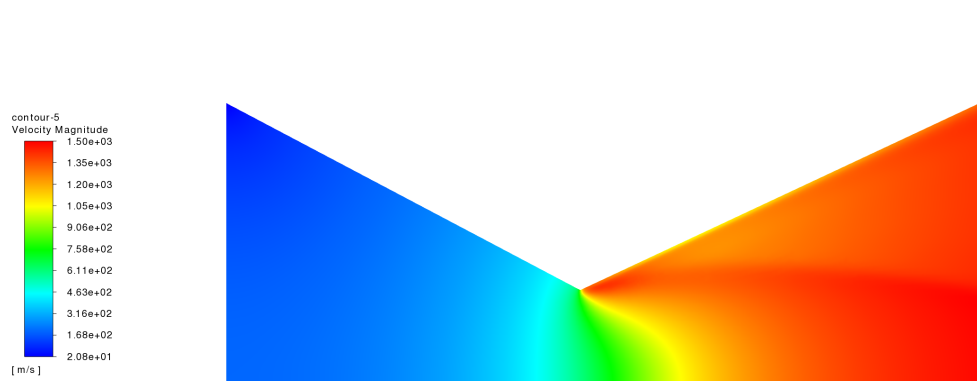
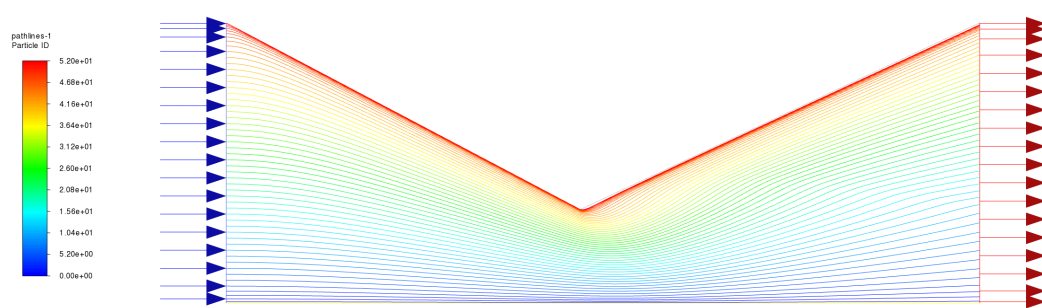


Figure 85 – Density Field for the inviscid simulation of the Conical-Shaped Nozzle



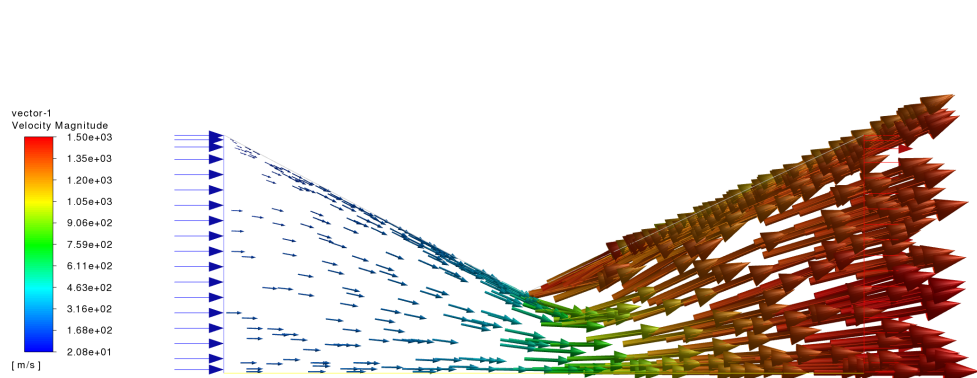
ANSYS
2021 R1
ACADEMIC

Figure 86 – Velocity Field for the inviscid simulation of the Conical-Shaped Nozzle



ANSYS
2021 R1
ACADEMIC

Figure 87 – Velocity Path-lines for the inviscid simulation of the Conical-Shaped Nozzle



ANSYS
2021 R1
ACADEMIC

Figure 88 – Velocity Vector Field for the inviscid simulation of the Conical-Shaped Nozzle

10.2.2 Viscous

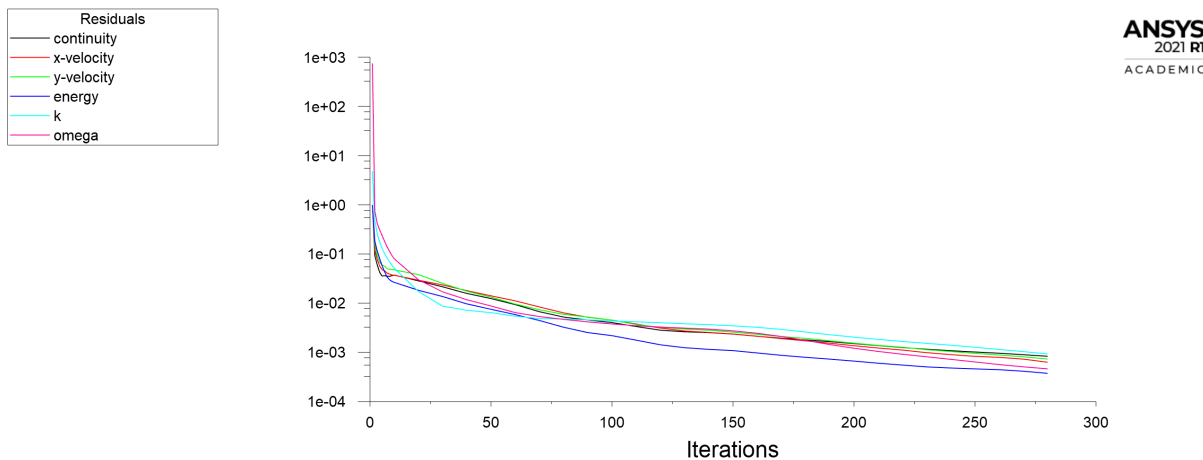


Figure 89 – Residuals for the Viscous simulation of the Conical-Shaped Nozzle

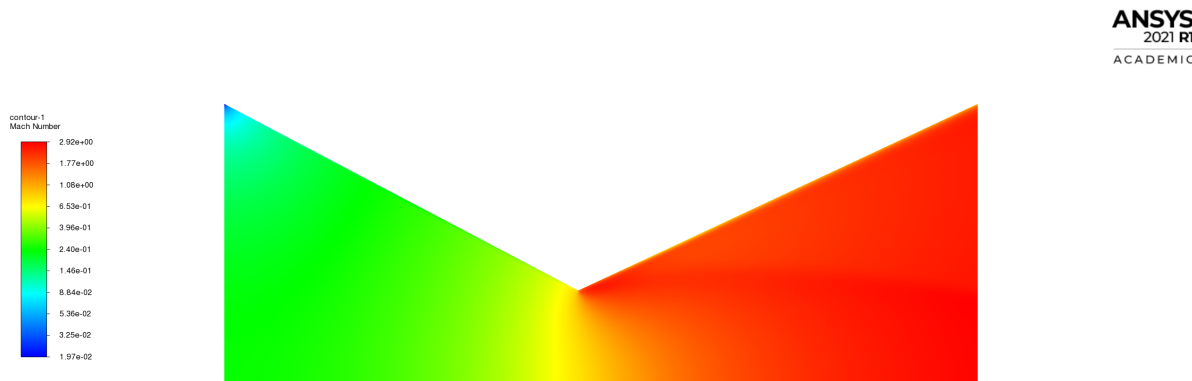


Figure 90 – Mach Number Field for the Viscous simulation of the Conical-Shaped Nozzle

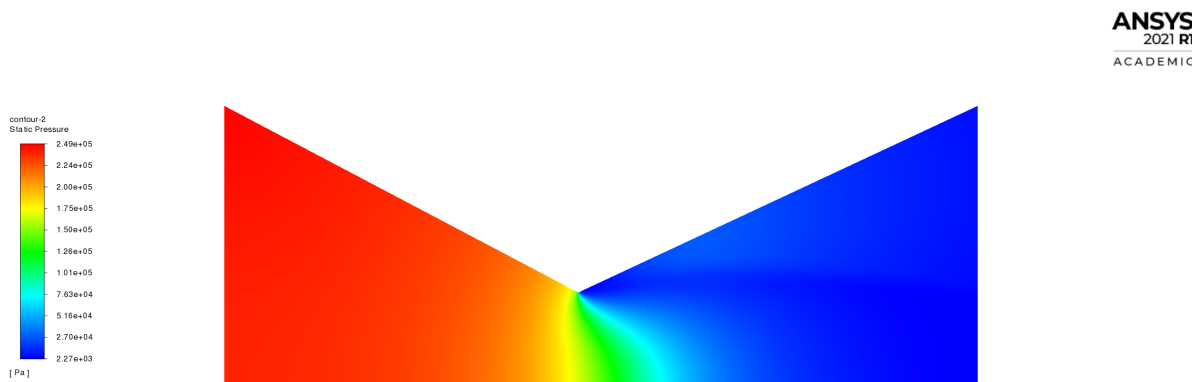


Figure 91 – Pressure Field for the Viscous simulation of the Conical-Shaped Nozzle

ANSYS
2021 R1
ACADEMIC

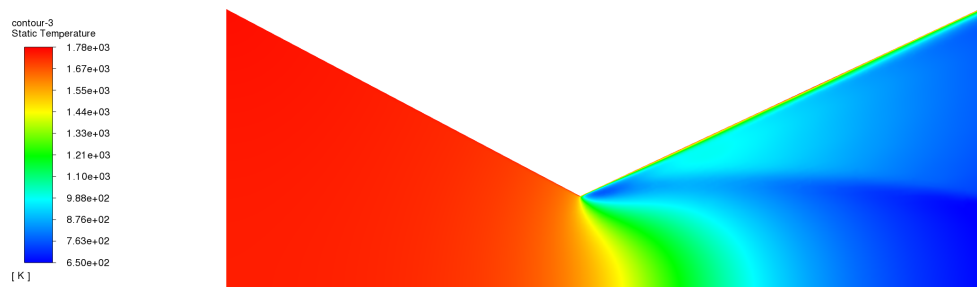


Figure 92 – Temperature for the Viscous simulation of the Conical-Shaped Nozzle

ANSYS
2021 R1
ACADEMIC

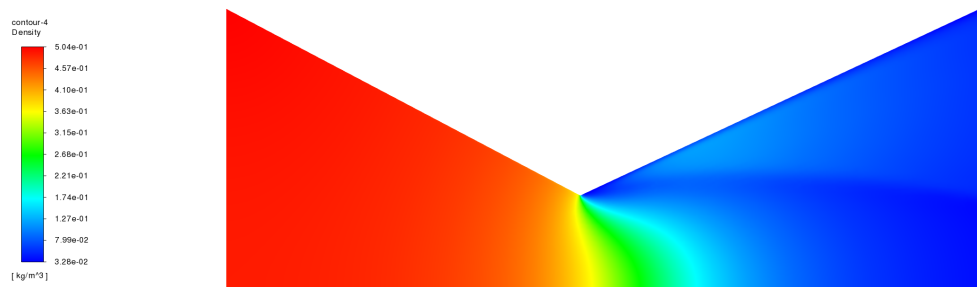


Figure 93 – Density Field for the Viscous simulation of the Conical-Shaped Nozzle

ANSYS
2021 R1
ACADEMIC

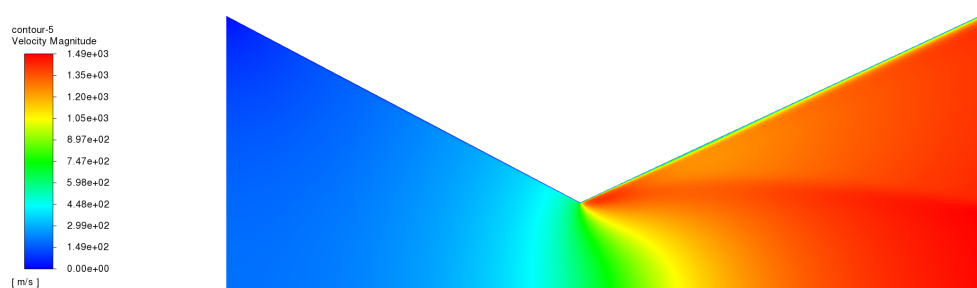
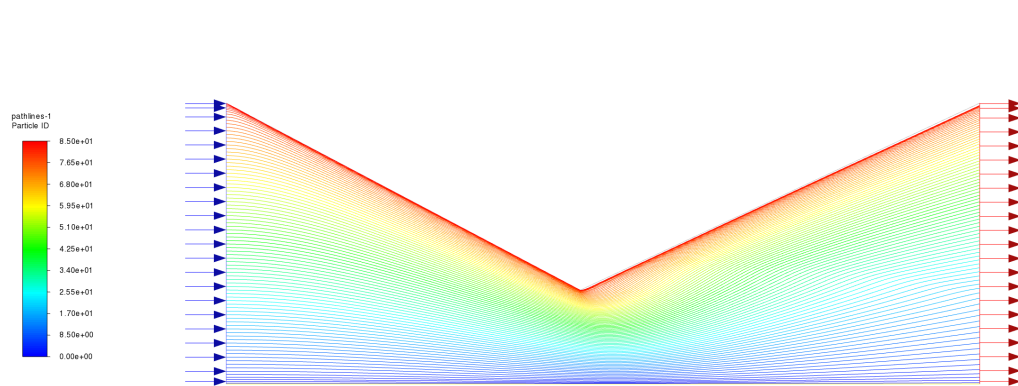
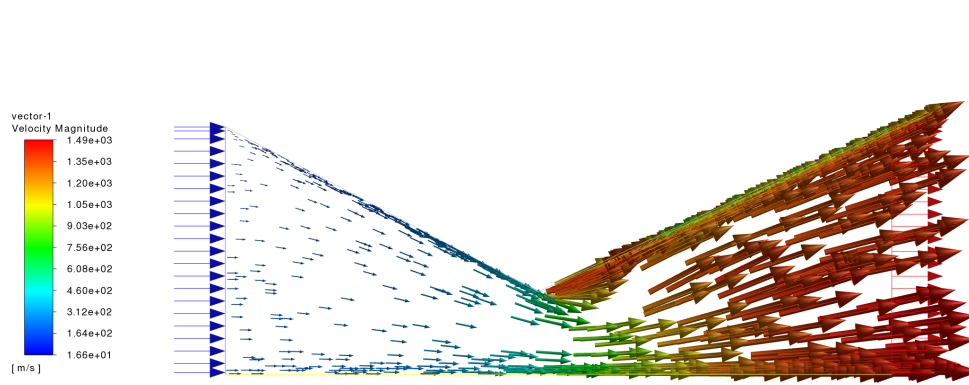


Figure 94 – Velocity Field for the Viscous simulation of the Conical-Shaped Nozzle



ANSYS
2021 R1
ACADEMIC

Figure 95 – Velocity Path-lines for the Viscous simulation of the Conical-Shaped Nozzle



ANSYS
2021 R1
ACADEMIC

Figure 96 – Velocity Vector Field for the Viscous simulation of the Conical-Shaped Nozzle

11 Discussion of Results of Part II

The properties discussed in (TORRES, 2021) from the inlet of the nozzle through its range will be compared in the following sections (Stations 5 to 7).

The results presented in Figures 22 to 43 show us the expected behavior calculated analytically. From the perspective of numerical results, Tables ?? to ?? will help us with the comparison.

11.1 Bell-Shaped

Mach Number

Parameter Station	Theoretical	Inviscid	$\varepsilon_{Inviscid}$ %	Viscous	$\varepsilon_{Viscous}$ %
5	0.20	0.1930	3.5000	0.1955	2.2500
6	1.00	1.0242	2.4200	1.0242	2.4200
7	2.65	2.5433	4.0264	2.6176	1.2226

Table 9 – Results of Mach Number for each station and errors

Pressure

Parameter Station	Theoretical	Inviscid	$\varepsilon_{Inviscid}$ %	Viscous	$\varepsilon_{Viscous}$ %
5	242466.60	242563.93	0.0400	242375.70	0.0372
6	131154.41	124944.32	4.7345	125665.5	4.1851
7	11603.08	10960.53	5.5417	11170.52	3.7318

Table 10 – Results of static Pressure for each station and errors

Temperature

Parameter Station	Theoretical	Inviscid	$\varepsilon_{Inviscid}$ %	Viscous	$\varepsilon_{Viscous}$ %
5	1760.92	1747.67	0.7524	1747.28	0.7746
6	1519.05	1455.60	4.1769	1455.20	4.2033
7	748.59	785.81	4.9720	762.9222	1.9215

Table 11 – Results of Temperature for each station and errors

Density

Parameter Station	Theoretical	Inviscid	$\varepsilon_{Inviscid} \%$	Viscous	$\varepsilon_{Viscous} \%$
5	0.48	0.4944	3.9583	0.4942	2.9583
6	0.31	0.3107	2.2581	0.3126	0.8387
7	0.06	0.0625	4.1670	0.0627	4.5000

Table 12 – Results of Density for each station and errors

Velocity

Parameter Station	Theoretical	Inviscid	$\varepsilon_{Inviscid} \%$	Viscous	$\varepsilon_{Viscous} \%$
5	166.95	161.70	3.1447	163.7459	1.9192
6	784.60	780.83	0.048	780.6959	0.4976
7	1459.85	1394.12	4.5025	1409.5990	3.4422

Table 13 – Results of Velocity for each station and errors

11.2 Conical-Shaped Nozzle**Mach Number**

Parameter Station	Theoretical	Inviscid	$\varepsilon_{Inviscid} \%$	Viscous	$\varepsilon_{Viscous} \%$
5	0.20	0.1901	4.950	0.1894	5.3000
6	1.00	0.9742	2.58	0.9702	2.98
7	2.65	2.6391	0.4113	2.6163	1.2717

Table 14 – Results of Mach Number for each station and errors

Pressure

Parameter Station	Theoretical	Inviscid	$\varepsilon_{Inviscid} \%$	Viscous	$\varepsilon_{Viscous} \%$
5	242466.60	242369.46	0.5064	247957.79	2.2647
6	131154.41	136821.65	4.3210	136542.03	4.1082
7	11603.08	12162.03	4.8173	12110.81	4.3758

Table 15 – Results of static Pressure for each station and errors

Temperature

Station \ Parameter	Theoretical	Inviscid	$\varepsilon_{Inviscid} \%$	Viscous	$\varepsilon_{Viscous} \%$
5	1760.92	1747.25	0.7763	1747.48	0.7632
6	1519.05	1477.87	2.7109	1479.64	2.5943
7	748.59	738.17	1.3919	748.16	0.0574

Table 16 – Results of Temperature for each station and errors

Density

Station \ Parameter	Theoretical	Inviscid	$\varepsilon_{Inviscid} \%$	Viscous	$\varepsilon_{Viscous} \%$
5	0.48	0.4941	2.9375	0.4943	2.9792
6	0.31	0.3187	2.8064	0.3198	3.1619
7	0.06	0.0569	5.1667	0.0570	5.0000

Table 17 – Results of Density for each station and errors

Velocity

Station \ Parameter	Theoretical	Inviscid	$\varepsilon_{Inviscid} \%$	Viscous	$\varepsilon_{Viscous} \%$
5	166.95	159.1802	4.6540	157.77	5.4987
6	784.60	748.2736	4.6300	745.86	4.9375
7	1459.85	1433.2916	1.8193	1426.23	2.3030

Table 18 – Results of Velocity for each station and errors

From the perspective of the graphs, the behavior of over-expansion of the wave was not expected, but all the values obtained from the surface integrals give us some values closer to the predicted from the analytical results, with margin of error being less than 6%. With respect to the residuals, great results were obtained and all the geometries converged. An interesting point is the fact for the conical shaped nozzle, there was a region of re-circulation for the flow next to the inlet, since the velocity vector had to adapt to the punctual change in the border of the wall.

Relative to the viscous flow, the boundary layer present in the models were almost not noticeable, and appeared significantly only on the temperature field.

From the perspective of comparison between both geometries, the bell-shaped nozzle had a better performance due to the transition to supersonic flow was less intensive than in the case of the conical.

12 Conclusion

A general good result was obtained from the simulations presented in this work. All properties had an expected behavior from what was provided by theory.

In the case of the comparison, what could be observed was that the bell-shaped geometry had the main advantage. First, the changing flow properties from subsonic to supersonic are way more smoother inside the transonic region when compared with the behavior inside conical-shaped.

All in all, the design of a bell-shaped nozzle can be more sophisticated than an older conical-shaped one.

For the purpose of this work, all knowledge developed was positive and a great amount of predictions by the analytical theory was made successfully.

References

LUIZ, F. *Avaliação da qualidade da malha*. 2015. [Online; accessed 14 May 2021]. Disponível em: <<http://notasemcfd.blogspot.com/2015/07/avaliacao-da-qualidade-da-malha.html>>. Cited in page 10.

TORRES, L. de J. Analytical calculations for a supersonic diffuser and nozzle. University of Brasilia, 2021. Cited 7 times in pages 5, 6, 26, 29, 30, 31, and 51.